Exploring the Adsorption Mechanism of Novel Biscoumarin Derivatives as Corrosion Inhibitors for Stainless Steel in 2 M H₂SO₄ Medium: An Integrated Approach Combining Electrochemical and Theoretical Studies

Hoyam Chahmout[1] · Moussa Ouakki[1,2] · Fatima El Hajri[1] · Omar Dagdag[3] · Hansang Kim[3] · Zakaria Benzekri[1,4] · Elhachmia Ech-chihbi[5] · Avni Berisha[6] · Saïd Boukhris[1] · Mohammed Cherkaoui[1,2]

Abstract

This study investigates the inhibition effect of two newly synthesized biscoumarin compounds, (Z)-4-hydroxy-3-((4-hydroxy-2-oxo-2H-chromen-3(8aH)-ylidene)(phenyl)methyl)-2H-chromen-2-one (P1) and (Z)-3-((4-chlorophenyl)(4-hydroxy-2-oxo-2H-chromen-3(8aH)-ylidene)methyl)-4-hydroxy-2H-chromen-2-one (P2), on the corrosion behavior of stainless steel in a 2M H₂SO₄ solution. Various methods, including potentiodynamic polarization (PDP), electrochemical impedance spectroscopy (EIS), scanning electron microscopy coupled to energy-dispersive X-ray spectroscopy (SEM–EDX), as well as density functional theory (DFT), Monte Carlo simulation (MC) and molecular dynamics (MD), were used in this investigation. The electrochemical findings revealed that P1 and P2 exhibit mixed inhibition behavior. Higher inhibition efficiencies are achieved at higher concentrations of these compounds. Indeed, at a concentration of 10^{-3} M, the inhibition efficiency reached 99 and 99.5% for P2 and P1 respectively, although it decreased slightly with increasing temperatures. The adsorption of studied inhibitors followed the Langmuir adsorption isotherm model. In addition, SEM–EDX analysis of the steel surface revealed a protective layer formed by the adsorbed inhibitors. Furthermore, the theoretical methods (MC and MD) were consistent with the experimental data, confirming the obtained results.

Keywords Biscoumarin · Inhibition · Steel · Sulfuric acid · Impedance and theoretical simulations

1 Introduction

The study and understanding of corrosion in metallic materials is of paramount importance to the scientific community to prevent its economic and societal consequences [1]. According to the World Corrosion Organization, metal corrosion generates very costly waste every year, accounting for 3–4% of industrialized gross domestic product (GDP) and damaging a quarter of annual steel production [1]. In addition, the Moroccan Confederation for Anticorrosion Certification COMACAC has indicated that the cost of corrosion in Morocco is likely to represent 5% of the national GDP [2]. Metallic corrosion is an inherent electrochemical phenomenon that transforms metals and alloys

Hoyam Chahmout and Omar Dagdag have contributed equally to this work.

✉ Hansang Kim
hskim70@gachon.ac.kr

✉ Avni Berisha
avni.berisha@uni-pr.edu

1 Laboratory of Organic Chemistry, Catalysis and Environment, Faculty of Sciences, Ibn Tofaïl University, PO Box 133, 14000 Kenitra, Morocco

2 National Higher School of Chemistry, Ibn Tofail University, PO Box 133, 14050 Kenitra, Morocco

3 Department of Mechanical Engineering, Gachon University, Seongnam 13120, Republic of Korea

4 Laboratory of Heterocyclic Organic Chemistry, Department of Chemistry, Faculty of Sciences, Mohammed V University in Rabat, PO Box 1014, Rabat, Morocco

5 Euromed University of Fes (UEMF), Fes, Morocco

6 Department of Chemistry, Faculty of Natural and Mathematics Science, University of Prishtina, 10000 Prishtina, Kosovo

into more stable compounds, such as hydroxides, oxides, and sulfides upon exposure to water [3]. Due to its superior mechanical properties, stainless steel is commonly used in a wide range of industrial heating and cooling systems, including oil refineries, pharmaceutical industries, and power plants[4]. Acid solutions are widely used in industrial processes such as descaling, cleaning and pickling, and metals are frequently exposed to corrosive media such as HCl, H_2SO_4 and HNO_3 at temperatures ranging from 60 to 90 °C to remove unwanted limescale deposits. These aggressive acid solutions can cause severe damage to metal installations [5].

Several methods have been previously used for the protection of steel against corrosion, including alloying [6], organic coatings [7, 8], anodization [9], conversion coatings [10], and the use of inhibitors [11, 12]. The usage of organic molecules has been discovered to be the most effective technique for preventing or reducing metallic corrosion in an aggressive environment [13].

Organic molecules containing heteroatoms such as N, S, O, or P, π electrons, or aromatic rings are frequently used to control metal corrosion in acidic environments [14, 15]. These compounds can interact with vacant d-orbitals of the metal by donating lone electron pairs from the heteroatoms, making them potential inhibitors [16, 17].

In acidic mediums, various types of heterocyclic compounds have demonstrated good corrosion inhibition behavior. Examples include phenyl-benzothiazole [18], quinoxaline [19], benzimidazole derivatives [20], indole derivatives [21] triazole [22], pyrrole [23], benzothiazine [24], and hydrazine [25].

Coumarin derivatives belong to a category of heterocyclic compounds characterized by multiple bonds, heteroatoms, and an aryl ring, making them well-suited as potential corrosion inhibitors. The coumarin family is one of the most widely employed natural chemical compounds globally. Coumarin serves as a versatile framework with a wide array of medicinal attributes and often acts as a foundational structure for creating novel and potent analogs with diverse physicochemical properties. This versatility is due to the ease of their synthetic transformation into various activated coumarin forms. Notably, the presence of substituents in the parent benzopyran moiety contributes to their distinctive properties [26, 27].

Both natural and synthetic coumarin derivatives exhibit a wide range of pharmacological and biological properties, including anti-inflammatory [28], anti-oxidant, [29], antitumor [30] burns, brucellosis, anti-coagulant, anti-bacterial, anticancer and anti-HIV [31]. In addition, several coumarin derivatives are used as flavoring and fixative agents, highlighting the environmentally friendly aspect of coumarin molecules [30]. Consequently, their synthesis has become a prominent and captivating subject of interest and research.

Based on previous research, the present study focuses on the investigation of newly synthesized bis(coumarin) compounds as corrosion inhibitors. In the present study, two bis(coumarin) compounds, namely P1 and P2, were synthesized and characterized by the method described El hajri et al. [30]. The investigated for their effect against the corrosion of stainless steel in 2M H_2SO_4 solution. Detailed studies were carried out using electrochemical analysis methods, including electrochemical impedance spectroscopy (EIS) and potentiodynamic polarization (PDP). In addition, SEM–EDX analysis was employed to examine the morphology of the adsorbed layer on the stainless steel surface. Computational studies such as Density Functional Theory (DFT), Monte Carlo simulation (MC) and molecular dynamics (MD) were used to confirmed the experimental results.

2 Experimental Conditions

2.1 Materials and Medium

Stainless steel with the following compositions C (0.04%), Si (0.41%), Mn (1.46%), P (0.07%), S (0.03%), N (0.08%), Cr (18.5%), Co (0.16%), Mo (0.33%), Ni (7.81%), Cu (0.51%) and Fe (balance) was used for the corrosion test. The test medium was made with a commercial solution of H_2SO_4 acid in both the presence and absence of the inhibitor.

Figure 1 depicts the molecular structures of the two examined substances (P1 and P2). For different experimental studies, stock solution of inhibitors was prepared using 2 ml of DMSO. In such medium, all tested compounds were fully soluble, with inhibitor C_{inh} spanning from 10^{-6} to 10^{-3} M.
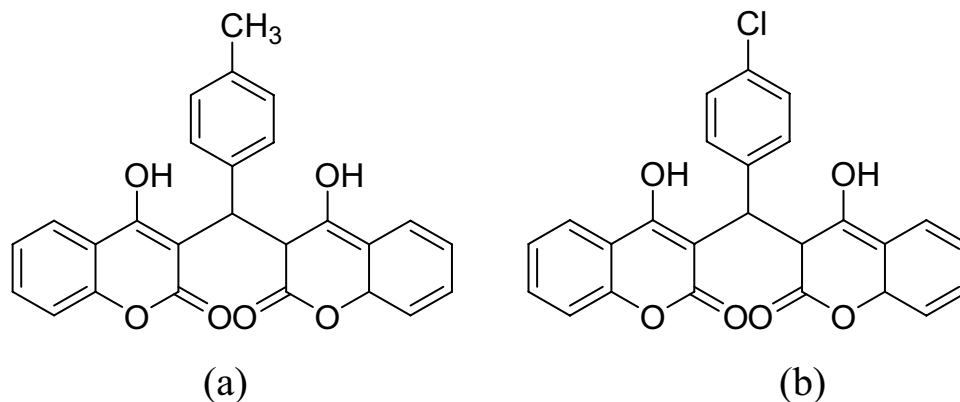
2.2 Electrochemical Study

Electrochemical experiments were carried out in a three-electrode Pyrex glass cell. The reference electrode (RE) used was a silver chloride electrode (Ag/AgCl), while a platinum plate served as the counter electrode (CE). A 1 cm^2 surface of S steel (face up) was used as the working electrode (WE). PDP and EIS tests were performed using a Potentiostat/Galvanostat/Voltalab PGZ100. Before each trace, the working electrode was immersed in the test solution for 30 min at the open-circuit potential to stabilize the system at a E_{ocp}.

PDP curves were generated by sweeping the electrode potential from – 900 to 300 mV relative to the corrosion potential at a sweep rate of 1 mV/s. The inhibition efficiency is evaluated using the following Eq. (1) [32]:

$$\eta_{pp}\% = \left[\left(i^{\circ}_{corr} - i_{corr} \right) / i^{\circ}_{corr} \right] \times 100 \tag{1}$$

Fig. 1 The examined substances' chemical structures: **a** P1 and **b** P2

(a)   (b)

where $i^{°}_{corr}$ and i_{corr} stand for the values of corrosion current densities in the absence and presence of inhibitor, respectively.

Electrochemical impedance measurements, on the other hand, were carried out in the frequency range of 100 kHz to 10 mHz using a sinusoidal perturbation potential of 10 mV amplitude. The corrosion inhibiting efficiency ($\eta_{imp}\%$) is calculated from the R_p values using the following Eq. (2) [33]:

$$\eta_{imp}\% = (R_p - R_p^{°}/R_p) \times 100 \tag{2}$$

$$\theta = R_p - R_p^{°}/R_p \tag{3}$$

where R_p^{0} and R_p indicate the polarization resistances in the absence and presence of inhibitor, respectively, and θ is the recovery rate Eq. (3).

2.3 SEM–EDX Analysis

The appearance of the metal surface when exposed to a 2M H_2SO_4 medium for 6 h before and after the addition of the two studied compounds was analyzed using SEM with a 20 kV acceleration voltage, and the surface composition was analyzed using the EDX technique.

2.4 Theoretical Investigations

DFT has become a widely adopted method for predicting the reactions of molecules with other substances or surfaces [34–36]. Due to its exceptional precision, the ab initio approach is widely employed [12, 13]. All quantum chemistry calculations involved full geometrical optimization using the Dmol3 module of the Biovia Materials Studio software package [37, 38]. Global optimizations are distinguished by the computation of vibration frequencies employing the DFT method are using the DFT method to produce the geometric structure of the desired compounds (using Dmol3, which included the G06/COSMO (water) model) [39].

MC simulation is widely used to study the interaction of a metal surface with a molecule inhibitor. This simulation is especially useful in elucidating a fundamental component of corrosion problems: the phenomenon of adsorption, which identifies the most stable adsorption sites on metal surfaces while expending the least energy [40–42]. Material Studio software is used to perform the MD and MC simulations using the adsorption locator and Forcite module [43]. This technique is primarily used to explore the interactions between inhibitor molecules and clean stainless steel surfaces under corrosive circumstances, to identify configurations with the lowest conformational energy. The adsorption of P1 and P2 inhibitors onto the iron surface is examined through MC and MD simulations conducted using Materials Studio 8.0 software [11, 44, 45]. We chose a highly stable surface, Fe (1 1 0), to replicate the adsorption process. The simulation box for MC and MD has dimensions of (24.823 752 Å × 24.823752 Å × 54.241658 Å). The MC simulations involved the continuous introduction of inhibitor molecules into the modeled cell, along with an aqueous solution containing corrosive species including H_2O (720), sulphate ions (05) and hydronium ions (10) [11, 46].

3 Results and Discussion

3.1 PDP Plots

To further understand the effect of produced biscoumarin derivatives on the electrochemical processes of metal surfaces, PDP plots of S-steel in 2M H_2SO_4 at varying P1 and P2 concentrations were performed. These curves are depicted in Fig. 2.

The results presented in Fig. 2 showed that the presence of the P1 and P2 inhibitors in the 2.0M H_2SO_4 solution affected the anodic reactions. Moreover, both P1 and P2 in the corrosive medium led to a significant reduction in the cathodic and anodic current densities (Fig. 2), with a more pronounced decrease observed as their concentration (C_{inh})
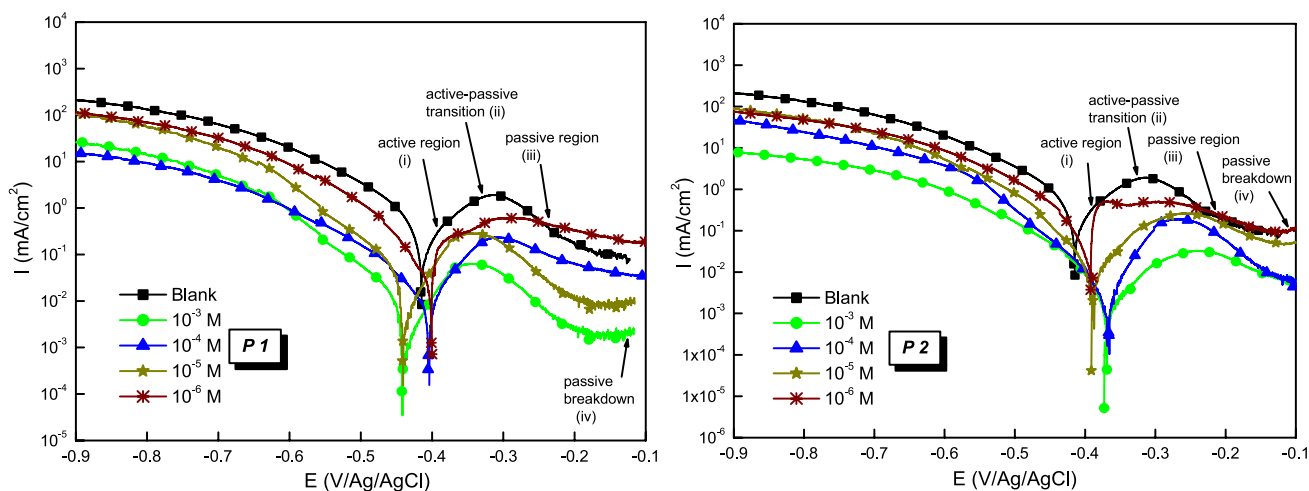
Fig. 2 Tafel plots for P1 and P2 biscoumarin derivatives

increased. Also, the values of the E_{corr} do not show significant shifts in the presence of the inhibitors. Therefore, it is not appropriate to classify compounds P1 and P2 as cathodic or anodic inhibitors. Consequently, the studied compounds can be classified as mixed-type inhibitors [47].

Tafel plots show that the hydrogen reduction mechanism happens according to a charge transfer mechanism, and the presence of biscoumarin molecules in 2M sulfuric acid solution does not cause any modification in the cathodic hydrogen evolution mechanism [48]. Because of its capacity to exist in a metastable state of passivity, S-steels offer good corrosion resistance in general. However, the passive layer gets degraded when S-steels are exposed to some corrosive medium rich in aggressive ions which causes the corrosion of steel [49]. The degradation of the passive layer occurs as a result of the controlled adsorption of aggressive ions at specific sites [50].

As shown in Fig. 2, the anodic branch can be identified by an active corrosion zone where there is a rise in i_{corr}, with the rising potential signifying the active dissolving of steel. Furthermore, beyond the active zone, the i_a decreases

to a critical level. This drop begins at roughly − 0.3 V and continues to − 0.1 V due to the creation of a passive layer on the surface of the S-steel.

However, it has been suggested that this film tends to partially decompose in an aggressive, ion-rich environment [51]. According to the polarization curve described, on the anodic leg, S-steel exhibits four regions: active (i), active–passive transition (ii), passive (iii), and passive breakdown (iv) [52]. Comparing the polarization plots of inhibitors P1 and P2 with those of blank, observations reveal that the introduction of inhibitors into the corrosive environment resulted in a significant reduction in i_a at the flat potential (primary passivation potential) and an expansion of the passivation zone. This suggests the development of a durable passive layer and, consequently, a reduction in localized corrosion [51]. Table 1 summarizes the electrochemical parameters obtained by extrapolation of the Tafel plots.

According to Table 1, the i_{corr} values decrease with the increase of concentrations ranging from (98 μA cm^{-2} at 10^{-6} M to 13 μA cm^{-2} at 10^{-3} M) for P2, and (95 μA cm^{-2} at 10^{-6} M to 8 μA cm^{-2} at 10^{-3} M) for P1 in 2M H$_2$SO$_4$,

Table 1 Electrochemical parameters extracted from Tafel plots of P1 and P2 (298 K)

Medium	Conc (M)	− E_{corr} (mV Ag^{-1} AgCl^{-1})	i_{corr} (μA cm^{-2})	− β_c (mV dec^{-1})	η_{PDP} %
Blank	–	411	828	134	–
P2	10^{-6}	392	98	131	88.1
	10^{-5}	389	55	133	93.3
	10^{-4}	370	22	129	97.3
	10^{-3}	364	13	127	98.4
P1	10^{-6}	397	95	134	88.5
	10^{-5}	437	67	132	91.9
	10^{-4}	404	18	130	97.8
	10^{-3}	439	08	126	99.0

and therefore the $\eta_{PDP}\%$ increases with increasing P1 and P2 concentrations, reaching a maximum value of 99% with compound P1. This may be due to the adsorption of P1 and P2 compounds on the surface of the S-steel, and blocks the active sites on the surface of this metal [53]. E_{corr} values obtained from Tafel slope plots in the presence and absence of inhibitors provide an excellent benchmark for determining the mechanism of inhibition. When the E_{corr} values are displayed within 85 mV on this, an inhibitor can be categorized as a mixed-type inhibitor. If the value of the inhibited material is higher than that of the blank, it is considered anodic; if it is lower, it is considered cathodic [54]. Table 1 demonstrates that the shift in E_{corr} values is below 85 mV for the two investigated inhibitor molecules. Consequently, the inhibitors can be characterized as mixed-type inhibitors.

Table 1 indicates that the presence of P1 and P2 slightly modifies the value of the cathodic Tafel slopes (β_c). However, the difference between the β_c values of inhibited and uninhibited systems is constant for different inhibitor concentrations. There is no discernible pattern in the β_c values of inhibited solutions as the concentration of the compounds studied increases. This suggests that the kinetics of cathodic reactions are not affected and that inhibition occurs by a simple geometric blocking mechanism [55].

3.2 EIS Diagrams

EIS is considered one of the most proven techniques for analyzing the surface characteristics of steel samples and the charge transfer process at the electrolyte/electrode interface. The EIS data have been represented in the form of a Nyquist diagram and are shown in Fig. 3.

Initial observations indicate consistent shape in the presence of inhibitors P1 and P2, compared to the blank solution, suggesting no alteration in the corrosion mechanism upon inhibitor addition at varying concentrations [56]. Figure 3 shows the presence of two semicircles for P1 and P2 at different concentrations, and their diameters correspond to the polarization resistance. The high-frequency capacitive loop primarily corresponds to the inhibitor film on the metal surface, while the low-frequency loop is typically associated with corrosion charge transfer and
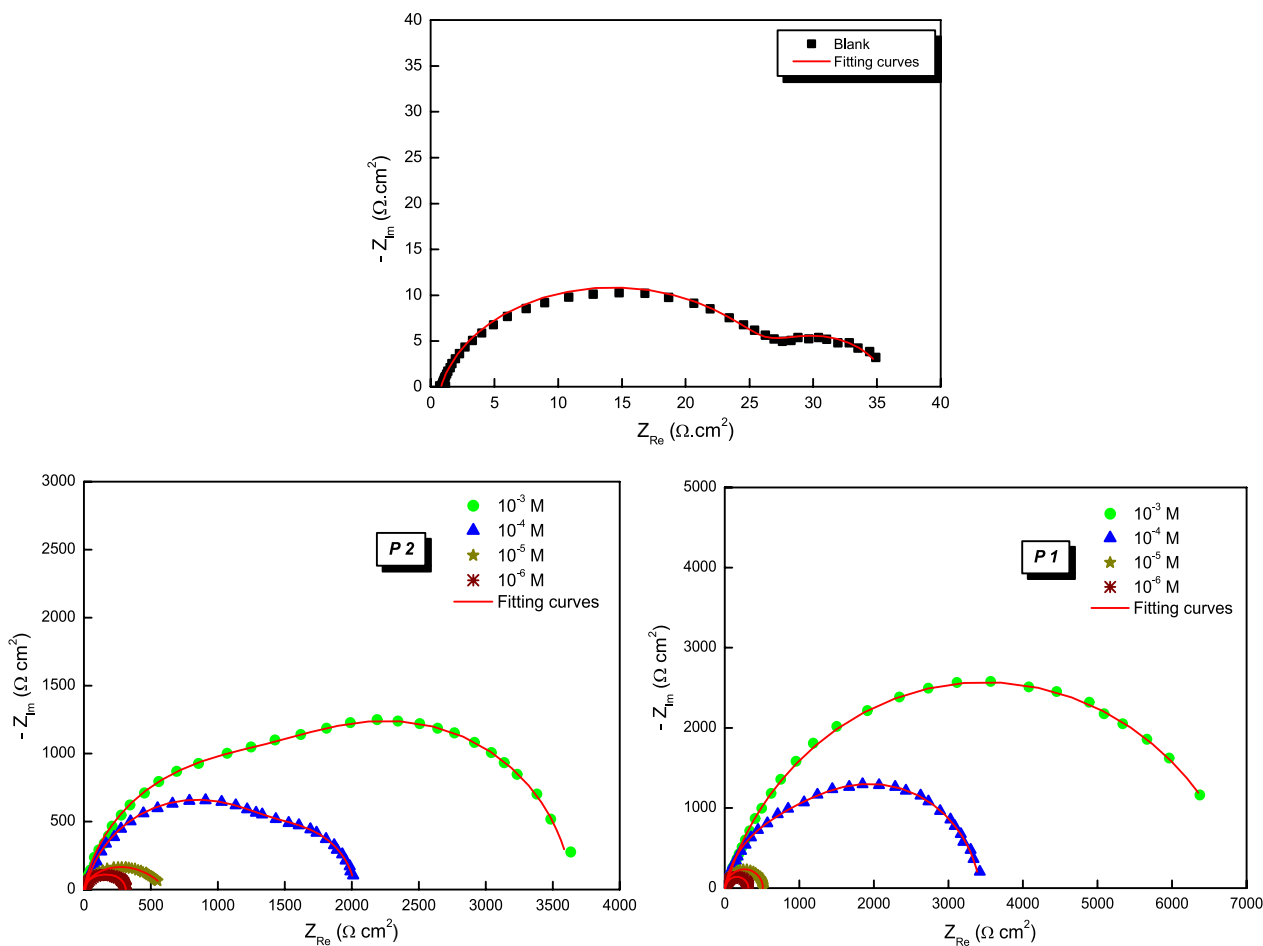

Fig. 3 Nyquist curves for P1 and P2 at 298 K

double-layer phenomena [57]. The diameters of the two depressed semicircles in the presence of the inhibitors are bigger than those reported for the blank solution, and they rise significantly when P1 and P2 concentrations increase. This is due to the formation of an inhibitor-adsorbed film on the metal's surface, which delays its contact with the acidic solution [58].

The equivalent circuit depicted in Fig. 4 serves to validate or refute mechanistic models and aids in determining electrochemical parameter values for the studied system [59, 60].

To replace an ideal capacitor, constant-phase elements (CPE) are utilized. This enables the description of the observed depression in the capacitive semicircle. The CPE is considered a versatile tool capable of describing the exponential distribution of electrochemical reaction parameters associated with charge and mass transfer energy barriers [61, 62]. The depression of the capacitive semicircle is attributed to surface heterogeneity, which can result from factors such as surface roughness, dislocations, active site distribution or inhibitor adsorption. The impedance of the CPE is shown as follows (Eq. 4) [63]:

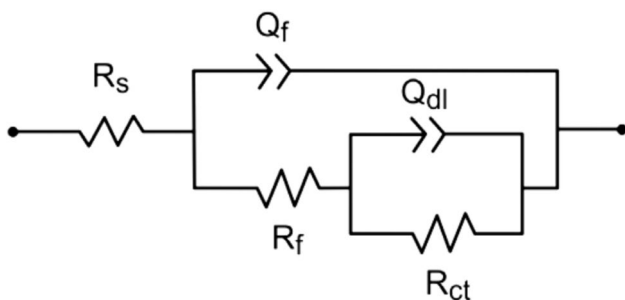$$Z_{CPE}(\omega) = Q^{-1}(j\omega)^{-n} \tag{4}$$

Fig. 4 Equivalent electrical circuit of metal/P1 and P2/H$_2$SO$_4$

where "Q" represents the coefficient of proportionality of the CPE, "j" is the imaginary number, "ω" corresponds to the angular frequency (in rad s^{-1}) and "n" can be utilized as a factor of surface homogeneity ($-1 \leq n \leq +1$).

Furthermore, the C_{dl} for a circuit containing a CPE is computed using the below Eq. (5) [64]:

$$C_{dl} = Q(2\pi w_{max})^{n-1} \tag{5}$$

where $w_{max} = 2\pi f_{max}$ and f_{max} is the frequency at the maximum value of the imaginary part of the impedance spectrum.

The EIS parameters calculated from the simulation of the impedance plot and η_{imp} (%) for the different C_{inh} of P1 and P2 in 2M H$_2$SO$_4$ medium are listed in Table 2.

The polarization resistance (R_p) of steel significantly increases in the presence of both inhibitors and further rises with higher concentrations, reaching its maximum values of 3651 Ω cm^2 for P2 and 6986 Ω cm^2 for P1 at 10^{-3} M. The adsorption of the two organic chemicals on the steel surface and the formation of a protective layer are responsible for the considerable increase in polarization resistance (R_p) [65]. On the other hand, the Q_f value diminishes as concentrations increase. This is likely due to the increase in double-layer thickness caused by the adsorption of organic molecules, which displaces H$_2$O molecules and corrosive ions at the steel/solution interface [66]. Nonetheless, an increase in n values with C_{inh} molecules is explained by a decrease in surface heterogeneity caused by the creation of adsorptive layers by the examined molecules [15]. Moreover, the values of n closely approach unity, signifying that the electric double layer in this study operated akin to a pseudo-capacitor [57]. The C_{dl} can be computed utilizing the subsequent Eq. (6) [67]:

$$C_{dl} = \frac{\varepsilon \cdot \varepsilon_0 \cdot s}{e} \tag{6}$$

where $\mathcal{E}$ and $\mathcal{E}_o$ represent the dielectric constants of the medium and permittivity under vacuum, e represents the

Table 2 Changes in kinetics for P1 and P2 at 298 K

Inhibiteur	Con M	R_s Ω cm^2	Q_f μFcm^2	n_f	R_f Ω cm^2	Q_{ct} μFcm^2	n_{ct}	R_{ct} Ω cm^2	R_p Ω cm^2	E%	θ
2.0 M H$_2$SO$_4$	–	0.9	798	0.896	25.4	447	1	10.6	36	–	–
P2	10^{-6}	0.8	694	0.875	226	346	0.894	66	292	87.6	0.876
	10^{-5}	0.5	552	0.895	143	266	0.705	478	621	94.2	0.942
	10^{-4}	1.0	165	0.865	1615	295	0.869	400	2015	98.2	0.982
	10^{-3}	0.4	159	0.878	2266	101	0.954	1385	3651	99.0	0.990
P1	10^{-6}	0.7	238	0.954	81	257	0.877	237	318	88.6	0.886
	10^{-5}	0.6	227	0.921	356	298	0.854	118	474	92.4	0.924
	10^{-4}	0.4	155	0.885	2184	142	0.958	1243	3427	98.9	0.989
	10^{-3}	1.0	255	0.797	482	27	0.931	6504	6986	99.5	0.995

thickness of the protective layer and S correspond to the electrode surface.

Figure 5 displays Bode Modulus and Bode angle plots for S-Steel in an H_2SO_4 medium, with and without different C_{inh} of the investigated inhibitors. In the Bode angle plots, we notice the presence of two peaks indicating two-time constants at the lower and the higher frequencies [68]. Furthermore, the phase angle values are elevated in the presence of the examined inhibitor compared to the corrosive medium. This result implies that a protective film forms on the surface of S-steel through inhibitor adsorption, causing the metal surface to become smoother [69].

The impedance within the low-frequency range $(10^{-1}–10^0 \text{ Hz})$ serves as an indicator of the metal's corrosion resistance: a higher impedance value corresponds to superior corrosion resistance. Figure 5 illustrates a significant rise in log|Z| values with increasing C_{inh} of the tested compounds, indicating effective corrosion inhibition. This affirms the robust adsorption of P1 and P2 molecules, leading to the creation of a protective, thin film on the surface of S-steel [70].

Table 3 summarizes some recent studies on the corrosion of steel metals using coumarin derivatives in acidic environments at a concentration of 10^{-4}M. A comparison with the coumarin molecules evaluated in this study indicates that the compounds studied exhibit higher inhibition efficiencies in terms of corrosion inhibition. Generally, these molecules are strongly adsorbed on the steel surface, effectively inhibiting the corrosion process.

3.3 Adsorption Isotherm Studies

Generally, the effectiveness of an inhibitor is determined by its ability to adsorb onto the steel surface, as well as the nature and chemical composition of its structure. Therefore, the adsorption isotherm provides crucial information for understanding the corrosion inhibition process and the interactions of the inhibitor molecules with the metal surface
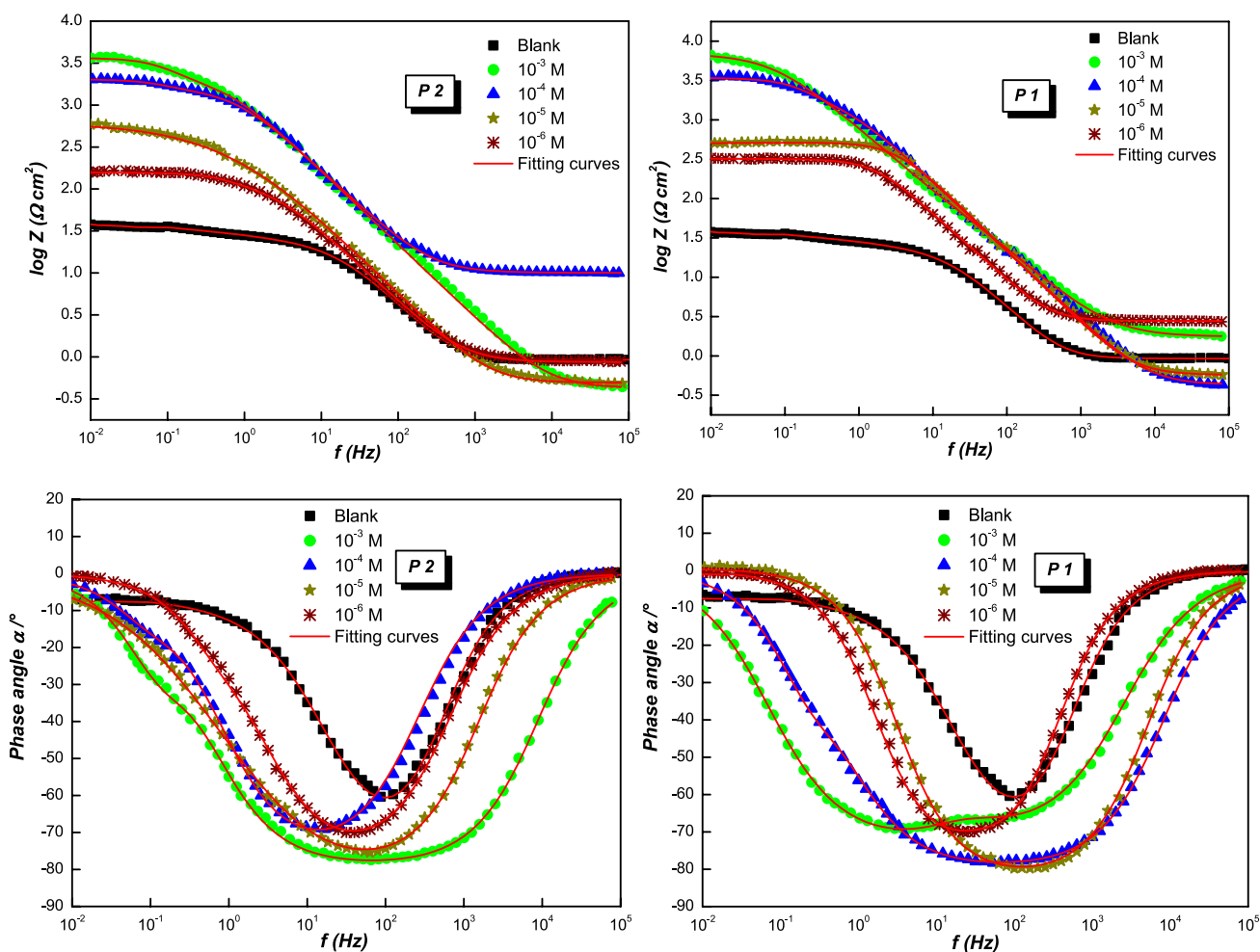

Fig. 5 Bode and phase angle curves for P1 and P2 at 298 K

Table 3 The inhibition efficiency of different coumarin molecules in an acidic environment
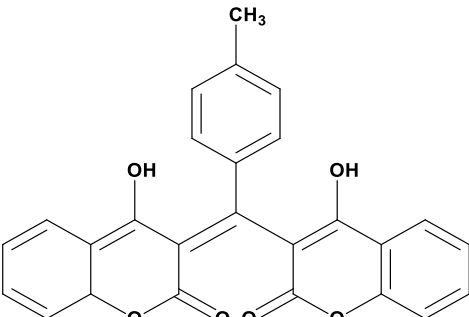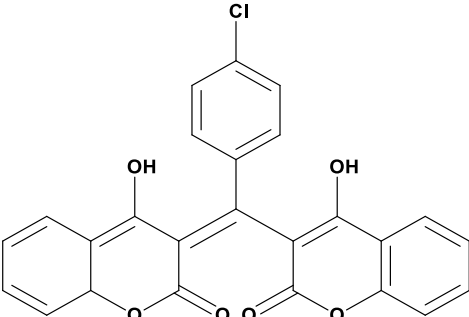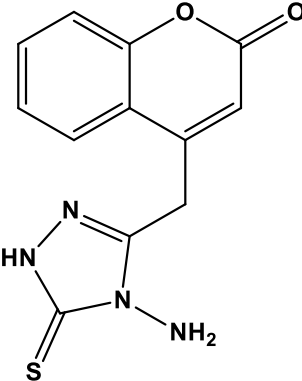
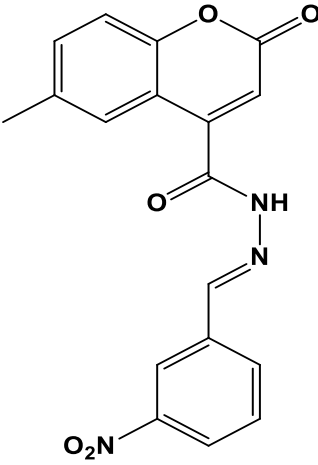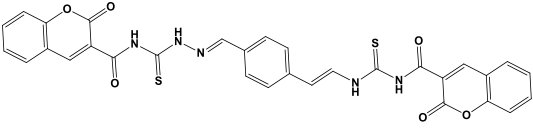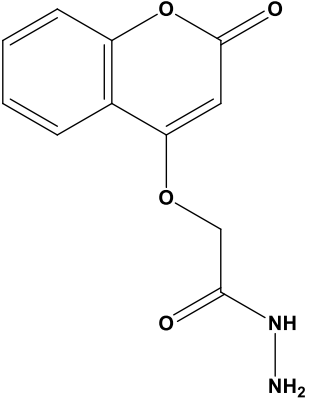| Chemical structure	C_{inh} (M)	η (%)	Metals	Corrosive solution	Reference
(Z)-4-hydroxy-3-((4-hydroxy-2-oxo-2H-chromen-3(8aH)-ylidene)(phenyl)methyl)-2H-chromen-2-one	10^{-4}	98.9	S-steel	2M H_2SO_4	This work
(Z)-3-((4-chlorophenyl)(4-hydroxy-2-oxo-2H-chromen-3(8aH)-ylidene)methyl)-4-hydroxy-2H-chromen-2-one	10^{-4}	98.2	S-steel	2M H_2SO_4	This work
4-((4-amino-1H-1,2,4-triazole-5(4H)-thione-3-yl)methyl) coumarin (ATMC)	10^{-4}	29%	M-steel	1M HCl	[71]

Table 3 (continued)
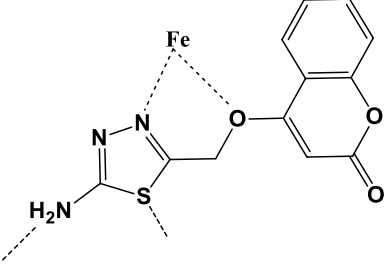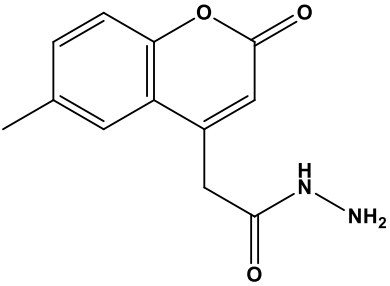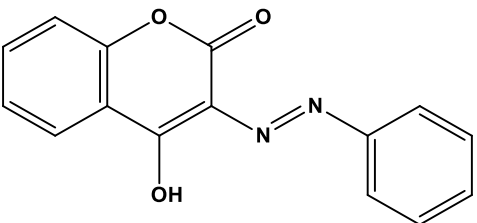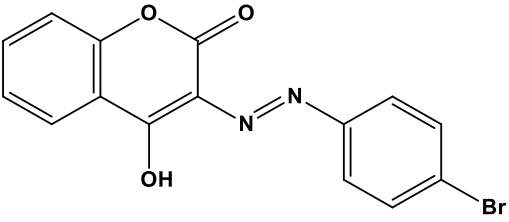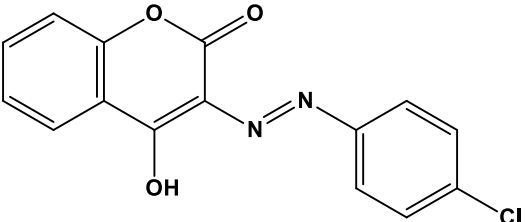
Chemical structure	C_{inh} (M)	η (%)	Metals	Corrosive solution	Reference
-(6-methylcoumarin-4-yl)- N´-(3-nitrobenzylidene)acetohydrazide (MCNAH	10^{-4}	21.5%	M-steel	1M HCl	[72]
N,N′-((2E,2′E)-2,2′-(1,4-phenylenebis(methanylylidene))bis(hydrazine carbono- thioyl))bis(2-oxo-2H-chromene-3-carboxamide) PMBH	10^{-4}	97.1	M-steel	1M HCl	[73]
2-(Coumarin-4-yloxy)acetohydrazide (EFCI)	10^{-4}	52	M-steel	1M HCl	[74]
4-[(2-amino-1, 3, 4-thiadiazol-5-yl)methoxy]coumarin (ATC)	10^{-4}	53	M-steel	1M HCl	[73]

Table 3 (continued)

Chemical structure	C_{inh} (M)	η (%)	Metals	Corrosive solution	Reference
 4-(6-methylcoumarin)acetohydrazide (MCA)	10^{-4}	56	M-steel	1M HCl	[74]
 (E)-4-hydroxy-3-(phenyldiazenyl)-2H-chromen-2-one (8)	10^{-4}	52	M-steel	1M HCl	[75]
 (E)-3-((4-bromophenyl)diazenyl)-4-hydroxy-2H-chromen-2-one (9)		65			
 (E)-3-((4-chlorophenyl)diazenyl)-4-hydroxy-2H-chromen-2-one (10)		57			

[75]. After assessing various isotherms like Frumkin, Temkin, Freundlich, and El-Awady, as shown in Fig. 6.

These isotherms allow us to connect the recovery rate to P1 and P2 concentrations using the formulas in Table 4, where f is the energy inhomogeneity factor. When this factor is positive ($f > 0$), the adsorbed species are attracted to one another laterally; when it is negative ($f < 0$), the opposite is true. "n" is the adsorption intensity, "K_{ads}" is the equilibrium constant of the adsorption processes, C_{inh} is the concentration of the products under examination, and θ is the rate at which an adsorbed inhibitor covers the steel surface. Among the tested isotherms, Langmuir model was found to be the best adsorption model of the P1 and P2 molecules on the steel surface in 2.0 M H_2SO_4 medium, with R^2 values close to unity.

The Langmuir model suggests that the steel surface has a limited number of adsorption sites, each capable of supporting a single adsorbed molecule. Furthermore, adsorbed molecules are assumed to have no interactions with each other, and all adsorption sites are thermodynamically identical. As a result, the adsorption energy remains constant across all surface coverage rates θ, indicating a uniform distribution of energy on all sites [72, 76]. Consequently, the Temkin, Frumkin, and Freundlich models presuppose a non-ideal adsorption process. Additionally, the correlation factor coefficient values are extremely near to unity.

In the present investigation, the parameter "f" of the Frumkin isotherm and "f" of the Temkin isotherm are negative indicating the existence of a lateral attraction between the adsorbed species. Thus, the obtained value of
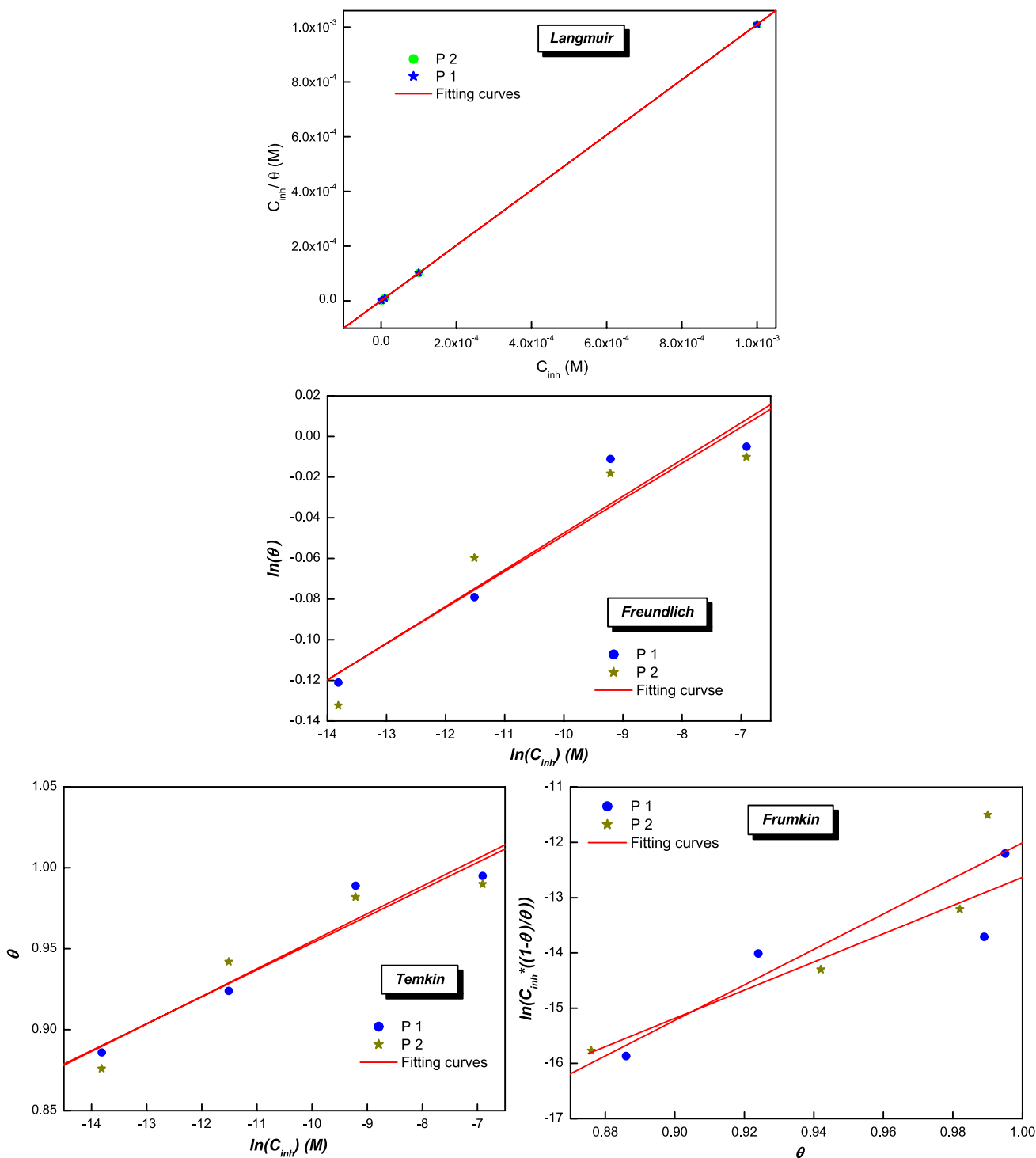
Fig. 6 Isothermal models tested to describe the adsorption of the two compounds onto S-steel in the examined medium at 298 K

n for Freundlich model is very different from the reference value of 0.6, which reveals that the adsorption mechanism studied cannot reasonably be modeled by the Freundlich isotherm, despite a value of R^2 in the standards [77, 78].

The K_{ads} and ΔG_{ads} parameters indicate the nature of the adsorption process and its spontaneity. According to Fig. 6, K_{ads} values were obtained from the reciprocal

Table 4 Adsorption parameters of P1 and P2 inhibitors

Isotherm	Linear form	Parameter	P1	P2
Langmuir	$k_{ads}c_{inh} = \frac{\theta}{1-\theta}$	R^2	1	1
		K_{ads} (L mol^{-1})	203.4×10^4	202.4×10^4
		Pente	1.0	1.0
		ΔG_{ads} **(KJ mol^{-1})**	− 46.0	− 45.9
Temkin	$e^{-2f\theta} = k_{ads}C_{inh}$	R^2	0.9616	0.94681
		K_{ads} (L mol^{-1})	1.1249	1.1194
		Pente ($-1/2f$)	0.01702	0.01659
		f	− 29.4	-30.1
Freundlich	$\theta = k_{ads}C_{inh}^n$	R^2	0.96137	0.94292
		K_{ads} (L mol^{-1})	0.13319	0.12878
		Pente (n)	0.01807	0.01775
Frumkin	$\frac{\theta}{1-\theta}e^{-2f\theta} = k_{ads}C_{inh}$	R^2	0.8938	0.93045
		K_{ads} (L mol^{-1})	− 38.18433	− 44.1556
		Pente ($-2f$)	25.55356	32.14747
		f	− 12.8	− 16.1

intercepts of adsorption isotherms, and the ΔG_{ads} are calculated using Eq. (7) [79]:

$$\Delta G_{ads} = -RTln(C_{solvent}K_{ads}) \tag{7}$$

where R stand for the universal gas constant, T denotes the temperature and $C_{solvent}$ represents the concentration of solvent "water" in solution equal to 55.5 mol l^{-1}. Table 4 presents the adsorption parameters of P1 and P2 obtained from Langmuir isotherm.

From the results in the table, we observe a strong R^2 for both products, and the slope is very close to unity. The high K_{ads} values observed for the two tested compounds in Table 4 indicate their strong adsorption to the steel surface. This is because the functional groups of these molecules contain many donor atoms, such as O and Cl. Negative ΔG_{ads} values indicate a spontaneous adsorption process and a long-lasting adsorbed layer on steel surfaces. According to the literature, when ΔGads values approach -20 kJ mol^{-1}, physical adsorption is mainly due to electrostatic interactions between charged molecules and the charged metal surface. However, values close to -40 kJ mol^{-1} indicate electron sharing or transfer between active sites of inhibitors and the vacant "d" orbitals of the metal, resulting in the formation of a coordination bond (covalent bond). This phenomenon is known as chemisorption [80]. The ΔG_{ads} values calculated for the P1 and P2 inhibitors are close to -40 kJ mol^{-1}. This suggests that the inhibitor molecules are adsorbed by chemisorption on the S-steel surface.

3.4 Temperature Effect

Temperature plays a key role in inhibitor activity. It can affect the interactions between metals and inhibitors in corrosive environments, as well as the inhibitory efficacy of an inhibitor. Furthermore, exposing a metal to an aggressive environment at elevated temperatures can lead to several problems, including dissolution of the metal, desorption of inhibitors and desorption of adsorbed molecules [81].

It is crucial to gain further insight into the type of adsorption and the behavior of the inhibitors at high temperatures. PDP curves were generated at various temperatures ranging from 298 to 328 K, both in the absence and presence of 10^{-3} M inhibitor, within an acidic medium of 2 M H$_2$SO$_4$. These PDP curves are illustrated in Fig. 7, while Table 5 presents the corresponding electrochemical parameters.

As depicted in Fig. 7, it becomes evident that with increasing temperature, the PDP curves shift towards higher i_{corr} values, regardless of the presence of P1 and P2 inhibitors. The data presented in Table 5 highlights that, whether in the absence or presence of inhibitors, a temperature shift from 298 to 328 K leads to an elevated i_{corr}. Nevertheless, the presence of the inhibitor results in a notably smaller increase in the corrosion current compared to the blank case. Therefore, these results show that the studied inhibitors preserve their inhibiting characteristics at all the temperatures studied. Concerning the inhibitory effectiveness, the calculated values of inhibition efficiency show a slight decrease with the temperature increasing from 98.4 to 91.2% for P2 and 99 to 93% for P1.

This phenomenon may be attributed to the desorption of the investigated molecule from the steel surface [82]. The decrease in inhibition efficiency with temperature has been elucidated by Ammar et al. [83] as a result of the Van der Waals interactions between the inhibitor and the metal surface. These bonds are highly sensitive to thermal agitation and are easily broken as the temperature increases.
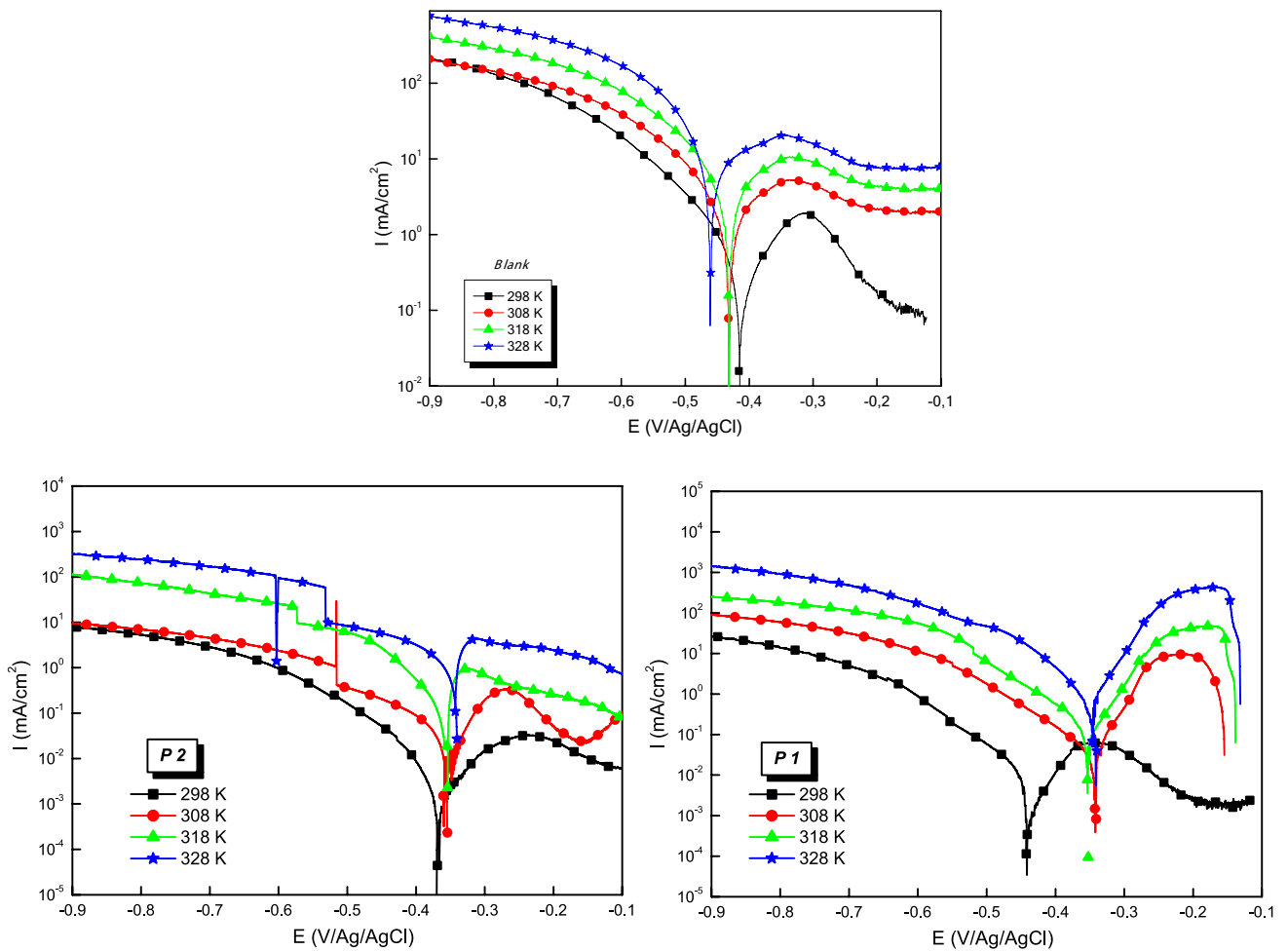
Fig. 7 PDP plots of S-steel in 2M.H$_2$SO$_4$ for P1 and P2 at different temperatures

Table 5 Various parameters related to changes in Tafel plots for P1 and P2 (10^{-3} M)

Medium	Tempe K	$-E_{corr}$ mV Ag^{-1} AgCl^{-1}	i$_{corr}$ μA cm^{-2}	$-\beta_c$ mV dec^{-1}	η_{PDP} %
Blank	298	412	827	135	–
	308	432	1490	139	–
	318	429	2409	142	–
	328	460	3250	153	–
P2	298	364	13	127	98.4
	308	350	48	134	96.7
	318	356	135	140	94.4
	328	338	284	148	91.2
P1	298	439	8	126	99.0
	308	340	35	137	97.6
	318	350	109	143	95.4
	328	348	226	150	93.0

Fig. 8 Variation of the %IE and temperature increase in $2M.H_2SO_4$ with the presence of $10^{-3}M$ inhibitors
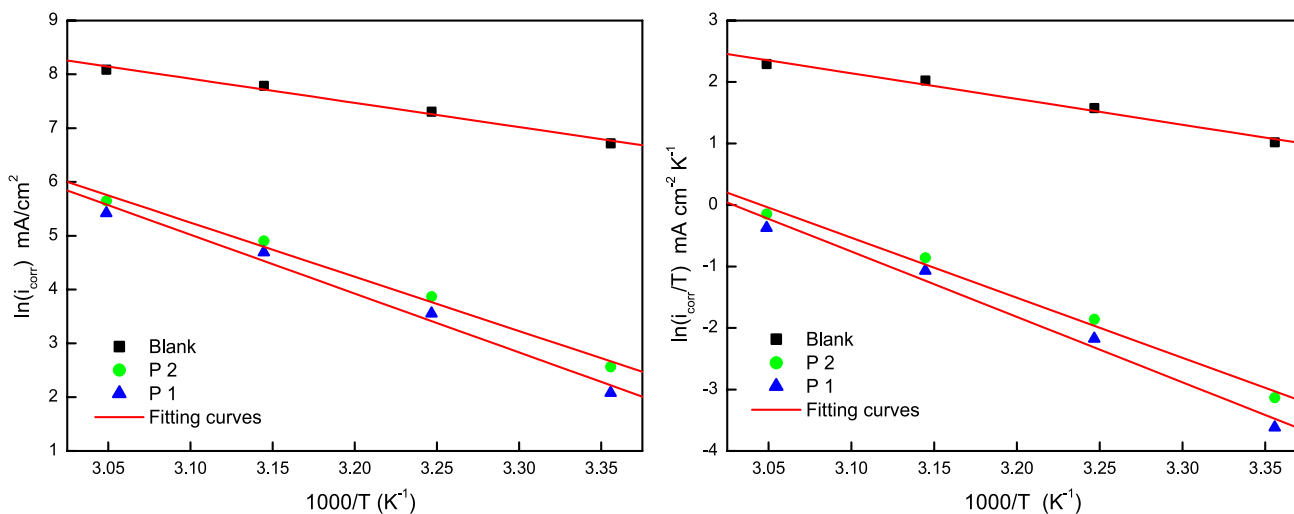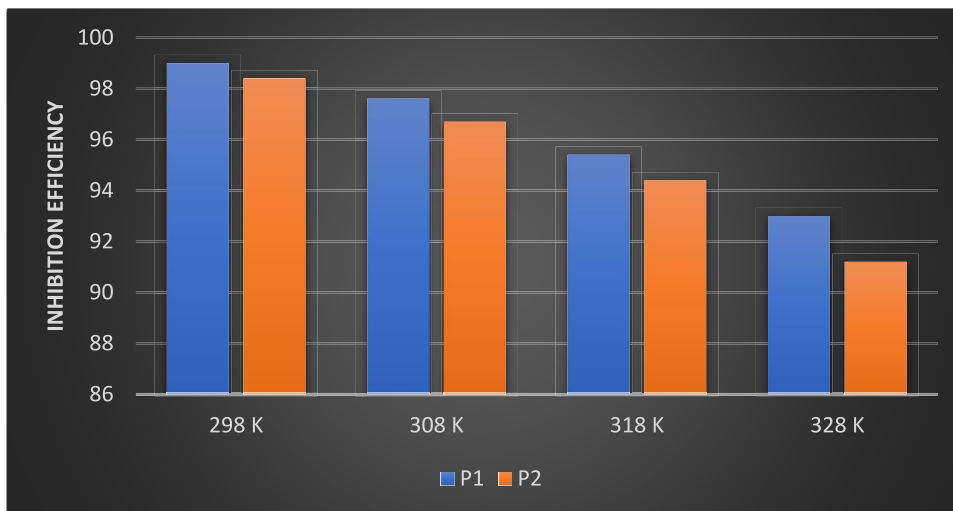

Fig. 9 Arrhenius and transition state curves for P1 and P2 (10^{-3} M)

Figure 8 shows the variation in η_{PDP} versus temperature at the optimum C_{inh} of 10^{-3} M for the two biscoumarin compounds (Fig. 8). It shows a slight decrease in efficiency with increasing temperature, and inhibitory characteristics do not change significantly.

3.5 Thermodynamic Parameters

By using the Arrhenius Equation, the E_a for the dissolution of S-steel in the presence and absence of an inhibitor in the corrosive medium 2.0 M H_2SO_4 was estimated from the i_{corr}, as follows Eq. (8):

$$i_{corr} = Ae^{\left(-\frac{E_a}{RT}\right)} \tag{8}$$

Table 6 Activation parameter values for P1 and P2 (10^{-3} M)

		E_a (kJ mol^{-1})	ΔHa (kJ mol^{-1})	ΔSa (kJ mol^{-1} K)
2.0M H_2SO_4	P2	83.8	81.2	49.8
	P1	91.0	88.4	70.3

Taking the logarithm of both sides of the Arrhenius Eq. (9) could be obtained

$$\ln i_{corr} = \ln A - \frac{E_a}{RT} \tag{9}$$

Additionally, using the transition state formula of the Arrhenius equation, the activation's entropy (ΔS_a) and enthalpy (ΔH_a) are determined as follows Eq. (10):

$$ln\left(\frac{i_{corr}}{T}\right) = \left[ln\left(\frac{R}{hN_a}\right) + \left(\frac{\Delta S_a}{R}\right)\right] - \frac{\Delta H_a}{RT} \tag{10}$$

where i_{corr} is the corrosion current density, A is the pre-exponential factor, h is the Planck's constant, N_a is the Avogadro's number, Ea is the apparent activation energy, R is the gas constant ($R = 8.314$ J mol^{-1} K^{-1}) and T is the absolute temperature.

Figure 9 depicts the variation of the ln (i_{corr}) and ln (i_{corr}/T) against 1000/T against 1000/T for S-steel in 2M H$_2$SO$_4$ electrolyte in the absence and presence of different C_{inh} values for P1 and P2. Table 6 displays the activation parameters that were derived from these two curves.

The formation of an energy barrier that slows the corrosion process can explain the increase in E_a values in the presence of P1 and P2 inhibitors. Therefore, the physisorption interaction between the organic molecule and the steel surface may be responsible for the higher E_a [84]. The positive standard activation enthalpy (ΔH_a) indicates the endothermic nature of the S-steel dissolution process, highlighting the resistance of steel to dissolution. The activation entropy values (ΔS_a) in the presence of P1 and P2 exhibit higher positive values when compared to the blank solution, indicating the ordering and disordering of inhibitor molecules on the S-steel surface. The increase in activation entropy when an inhibitor is present suggests that the adsorption of inhibitors and desorption of H$_2$O molecules result in increased entropy. Consequently, this enhances the disorder of P1 and P2 molecules during their adsorption onto the stainless steel surface [85].

3.6 Surface Analysis by SEM–EDX

Electrochemical measurements should be used to verify the results; the surface morphology of S-steel has been evaluated using SEM–EDX technique. Figure 10 shows the SEM images of S-steel in 2M H$_2$SO$_4$ before and after the addition of 10^{-3} M of P1 and P2 compounds. The comparison of SEM images reveals that the samples corroded significantly following immersion in the blank solution. We can see corrosion products forming across the entire surface of the material, and the metal surface becomes rough and cracked,
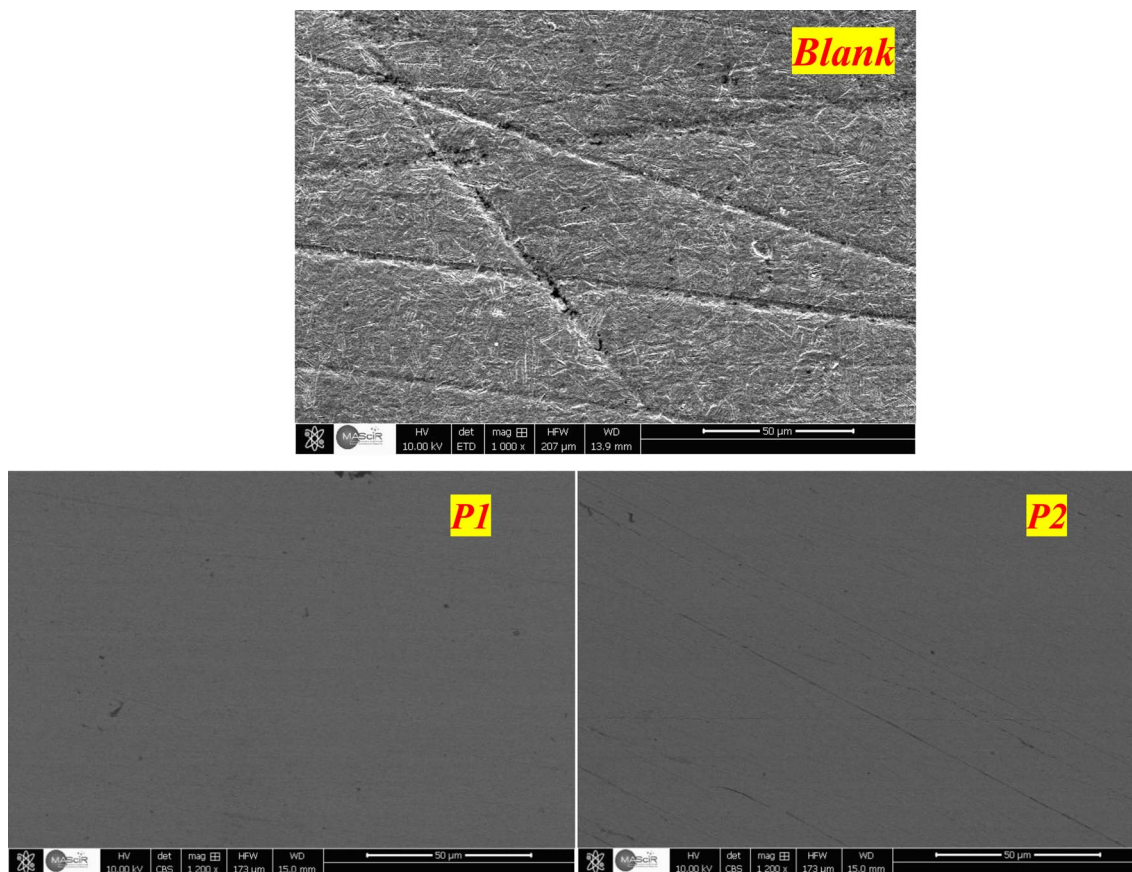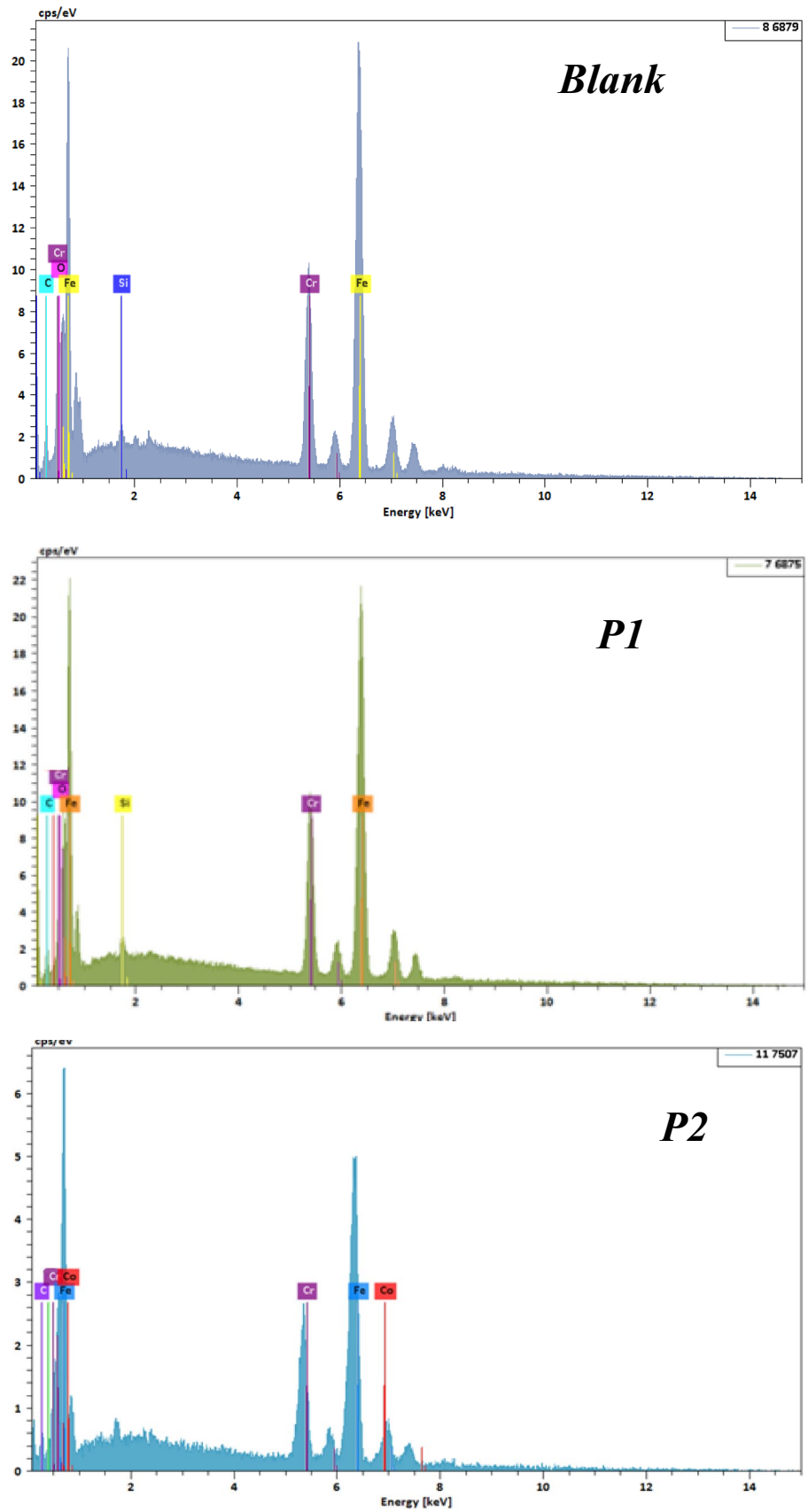

Fig. 10 SEM images of the uninhibited and inhibited samples for P1 and P2 at a concentration of 10^{-3} M for 6 h at 298 K

Fig. 11 EDX spectra (uninhibited and inhibited) for P1 and P2 at 10^{-3} M

with pits and cracks spaced arbitrarily apart. These results are frequently associated with the direct attack of sulfuric acid on steel surfaces. On the other hand, the addition of P1 and P2 at appropriate concentrations improved the surface morphology of S-steel. SEM micrographs reveal that, in the presence of both chemicals, the metal surface is devoid of corrosion products and becomes smoother, more homogeneous and brighter. This can be attributed to the formation of a thin protective film on the metal surface, which effectively prevents corrosion damage.

Moreover, to get more information about S-steel surface composition in the absence and presence of organic compounds, (EDX) analysis was used for steel samples. The EDX spectra for S-steel that was submerged for 6 h in a 2M H_2SO_4 solution, both with and without the addition of 10^{-3} M of P1 and P2, are shown in Fig. 11. The EDX spectra of S-steel in the blank display the distinctive peaks of several of the steel specimen's constituent elements (C, Mn, Cr, Si, and Fe). Also, the presence of a peak corresponding to Oxygen (O) confirms the formation of iron oxides in the corrosion process and the dissolution of the S-steel after immersion. However, EDX spectra in the presence of the inhibitor reveal the appearance of the distinctive Cl peak, which is present in the chemical composition of the organic molecule. In addition, a decrease in the intensity of oxygen peaks can be observed. These results confirm the
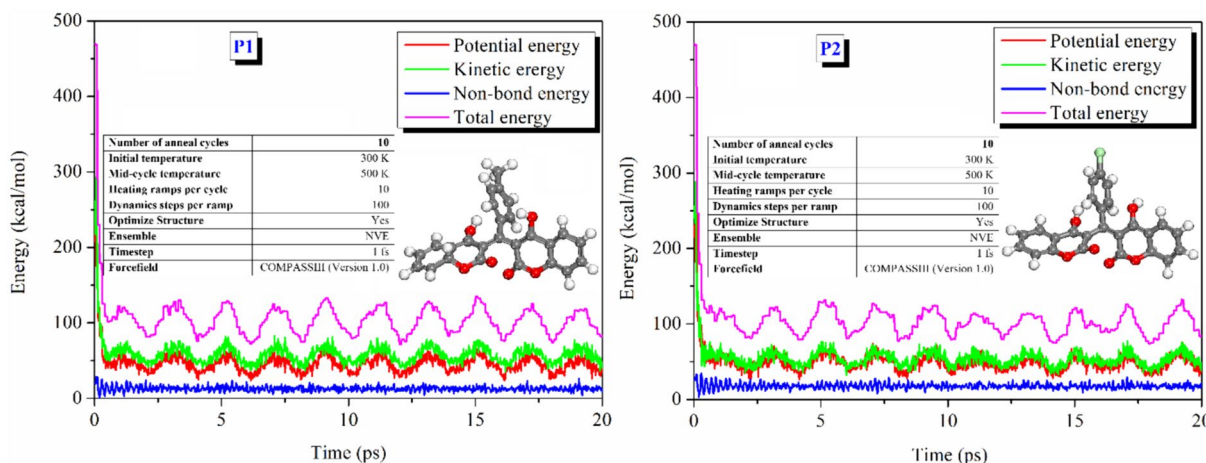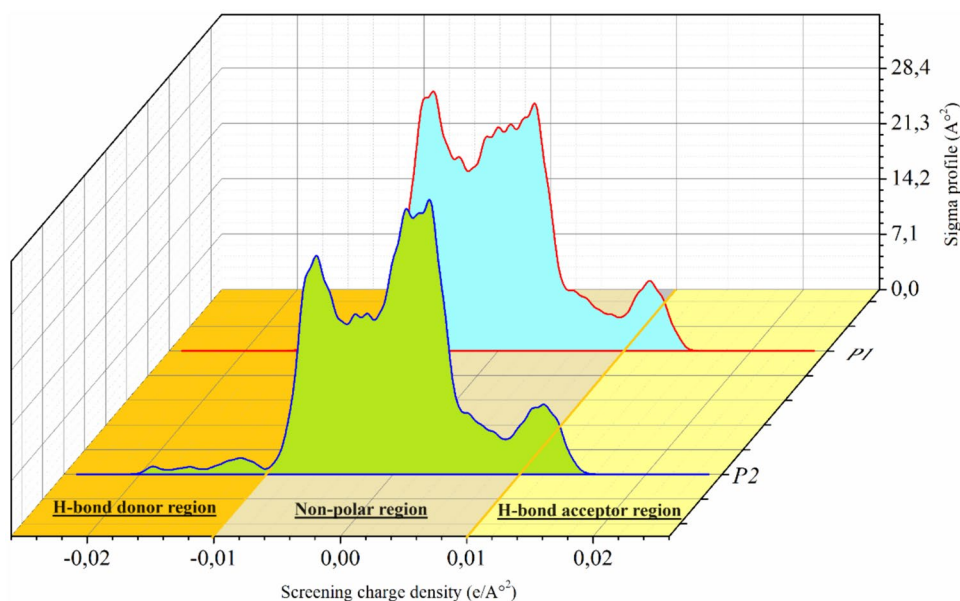

Fig. 12 Quench dynamic parameters and derived outputs

Fig. 13 σ-profile of the P1 and P2 inhibitors

development of a protective coating on the steel surface and the ability of chemicals to limit corrosion processes.

3.7 Theoretical Analysis

3.7.1 DFT Results

To expedite the DFT calculations and reduce computation time, a preliminary step was taken using the Quench method. This method involved utilizing the COMPASS III force field and the parameters listed in Fig. 12 to attain a low energy conformation of P1 and P2 inhibitors.

The COSMO model generates a sigma profile curve using charge density calculations, as seen in Fig. 13. Atomic nuclei in the COSMO model are slightly charged to represent their electrostatic potential [86]. The figure depicts the P1 and P2 inhibitors that can act as both an acceptor and a donor for hydrogen bonding. When put in a solution, water molecules form acceptor/donor interactions with the inhibitors, and the inhibitor's solubility is determined by its ability to form hydrogen bonds [86].

Theoretical studies offer valuable insights into the chemical activity of inhibitory compounds through electronic descriptors, which define the properties of these compounds and, consequently, elucidate the mechanisms of corrosion inhibition [87–89]. A higher E_{HOMO} value indicates enhanced electron donation, signifying improved corrosion inhibition efficacy as a result of increased adsorption of inhibitory molecules onto the S-Steel Surface. Furthermore, the least E_{LUMO} value indicates the ability to accept electrons from the metal surface [90, 91]. Furthermore, a lower value of the ΔE_{gap} represents the highest interaction of the metal/inhibitor and, as a result, a high protection effectiveness. The HOMO, LUMO and ESP surfaces of the P1 and P2 inhibitors are given in Fig. 14.

Table 7 Theoretical chemical characteristics for P1 and P2 inhibitors were calculated

Descriptor	P1	P2
HOMO	− 4.597	− 4.667
LUMO	− 3.556	− 3.623
ΔE_{gap}	1.041	1.044
I	4.597	4.667
A	3.556	3.623
χ	4.076	4.145
η	0.520	0.522
σ	1.923	1.915
ΔN	0.715	0.646
$\Delta E_{back-donation}$	− 0.130	− 0.130

According to the plots, the FMOs (HOMOs/LUMOs) orbitals for the P1 and P2 are found throughout the molecules, primarily on the aromatic doublets, the hydroxyl and oxo groups. These sites are responsible for electron donation and/or acceptance from the metal surface [92]. Additionally, the areas with a red color in the MEP indicate a negative electrostatic potential, with prominent concentrations around the –O–C=O linkages, as depicted in Fig. 14.

Table 7 lists the various quantum chemistry characteristics for the P1 and P2 inhibitors. According to Table 7, the HOMO of both P1 and P2 inhibitors is as follows: P1 > P2, which reflects that P1 has favorable electron-donating characteristics to the metal surface. As seen also in Table 7, the theoretical order of ΔE_{gap} and η is P1 < P2, suggesting that P1 has high electron-donating capabilities on the surface [17, 93].

The condensed Fukui index (FI) analysis was used to identify the inhibitors' local reactive sites. By analyzing the nucleophilic and electrophilic properties of the P1 and P2 inhibitors, the activity of the P1 and P2 inhibitors

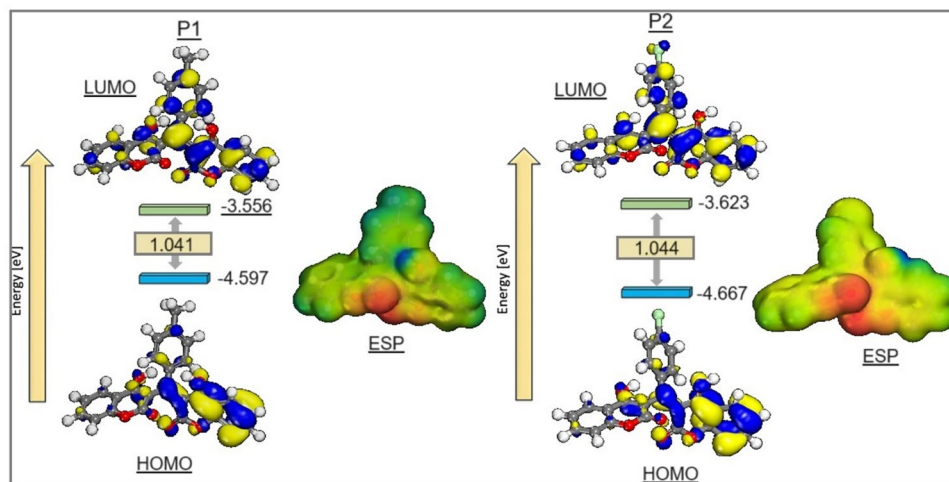**Fig. 14** HOMO, LUMO and ESP surfaces of the P1 and P2 inhibitors

Table 8 f_k^+ and f_k^- indices based on the Mulliken and Hirshfeld charges methods P1 and P2 inhibitors

Atom	P1				Atom	P2			
	f_k^+		f_k^-			f_k^+		f_k^-	
	Mulliken	Hirshfeld	Mulliken	Hirshfeld		Mulliken	Hirshfeld	Mulliken	Hirshfeld
C (1)	0.015	0.018	0.015	0.019	C (1)	0.015	0.018	0.015	0.018
C (2)	0.018	0.020	0.018	0.019	C (2)	0.018	0.019	0.017	0.019
C (3)	− 0.014	0.007	− 0.014	0.007	C (3)	-0.011	0.008	-0.010	0.008
C (4)	0.018	0.020	0.017	0.019	C (4)	0.017	0.019	0.016	0.018
C (5)	0.015	0.018	0.015	0.019	C (5)	0.015	0.018	0.015	0.018
C (6)	0.021	0.027	0.020	0.026	C (6)	0.018	0.025	0.018	0.024
C (7)	− 0.002	0.007	− 0.002	0.007	Cl (7)	0.041	0.038	0.042	0.039
C (8)	0.052	0.041	0.051	0.040	C (8)	0.054	0.041	0.053	0.040
C (9)	− 0.003	0.013	− 0.002	0.013	C (9)	-0.002	0.014	-0.001	0.014
C (10)	0.014	0.024	0.013	0.024	C (10)	0.013	0.024	0.013	0.024
C (11)	0.028	0.021	0.027	0.020	C (11)	0.028	0.020	0.027	0.020
O (12)	0.021	0.026	0.021	0.026	O (12)	0.020	0.026	0.021	0.026
C (13)	− 0.009	0.015	-0.009	0.015	C (13)	-0.008	0.015	-0.008	0.015
C (14)	0.035	0.036	0.035	0.037	C (14)	0.036	0.036	0.036	0.036
C (15)	0.026	0.028	0.026	0.028	C (15)	0.027	0.027	0.027	0.028
C (16)	0.032	0.028	0.031	0.027	C (16)	0.033	0.028	0.032	0.027
C (17)	0.007	0.012	0.007	0.012	C (17)	0.007	0.012	0.007	0.012
C (18)	0.015	0.015	0.015	0.015	C (18)	0.015	0.016	0.015	0.016
O (19)	0.014	0.016	0.015	0.016	O (19)	0.014	0.016	0.014	0.016
C (20)	0.016	0.013	0.016	0.013	C (20)	0.016	0.013	0.015	0.013
O (21)	0.041	0.040	0.042	0.040	O (21)	0.040	0.039	0.041	0.040
O (22)	0.030	0.028	0.031	0.029	O (22)	0.030	0.028	0.031	0.029
C (23)	0.021	0.020	0.020	0.020	C (23)	0.021	0.020	0.020	0.020
C (24)	0.011	0.017	0.011	0.017	C (24)	0.011	0.017	0.011	0.018
C (25)	0.020	0.024	0.020	0.024	C (25)	0.021	0.024	0.020	0.024
C (26)	0.013	0.016	0.014	0.016	C (26)	0.013	0.016	0.013	0.017
C (27)	0.049	0.048	0.049	0.048	C (27)	0.048	0.047	0.048	0.047
C (28)	0.017	0.031	0.017	0.031	C (28)	0.017	0.031	0.017	0.031
C (29)	0.050	0.058	0.051	0.058	C (29)	0.050	0.057	0.050	0.057
C (30)	0.029	0.036	0.029	0.036	C (30)	0.028	0.035	0.028	0.036
O (31)	0.029	0.028	0.029	0.029	O (31)	0.025	0.026	0.026	0.026
O (32)	0.025	0.024	0.025	0.024	O (32)	0.025	0.024	0.025	0.024
H (33)	0.017	0.011	0.017	0.010	H (33)	0.016	0.010	0.016	0.010
H (34)	0.019	0.011	0.019	0.011	H (34)	0.019	0.010	0.019	0.010
H (35)	0.019	0.011	0.019	0.010	H (35)	0.018	0.010	0.017	0.010
H (36)	0.017	0.011	0.017	0.011	H (36)	0.016	0.010	0.016	0.010
H (37)	0.011	0.007	0.011	0.007	H (37)	0.043	0.026	0.042	0.026
H (38)	0.013	0.009	0.013	0.009	H (38)	0.015	0.010	0.015	0.010
H (39)	0.009	0.006	0.009	0.006	H (39)	0.013	0.009	0.013	0.009
H (40)	0.045	0.028	0.044	0.028	H (40)	0.015	0.010	0.015	0.010
H (41)	0.015	0.010	0.015	0.009	H (41)	0.014	0.009	0.014	0.009
H (42)	0.015	0.008	0.013	0.009	H (42)	0.030	0.020	0.030	0.020
H (43)	0.013	0.010	0.015	0.010	H (43)	0.025	0.016	0.026	0.016
H (44)	0.014	0.009	0.014	0.009	H (44)	0.032	0.023	0.032	0.023
H (45)	0.031	0.020	0.031	0.021	H (45)	0.027	0.017	0.028	0.017
H (46)	0.026	0.016	0.026	0.016	H (46)	0.014	0.013	0.014	0.013
H (47)	0.033	0.023	0.033	0.023	H (47)	0.010	0.009	0.009	0.009
H (48)	0.029	0.018	0.029	0.018					

Table 8 (continued)

Atom	P1				Atom	P2			
	f_k^+		f_k^-			f_k^+		f_k^-	
	Mulliken	Hirshfeld	Mulliken	Hirshfeld		Mulliken	Hirshfeld	Mulliken	Hirshfeld
H (49)	0.013	0.011	0.013	0.011					
H (50)	0.010	0.009	0.010	0.009					

Fig. 15 MC and MD results derived from the adsorption configurations of P1 and P2 inhibitors
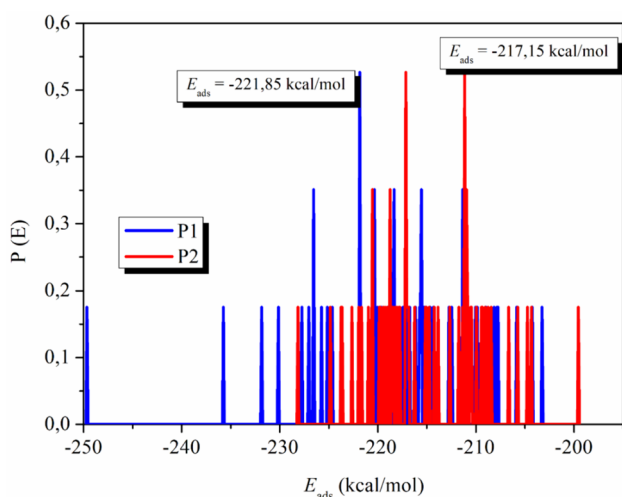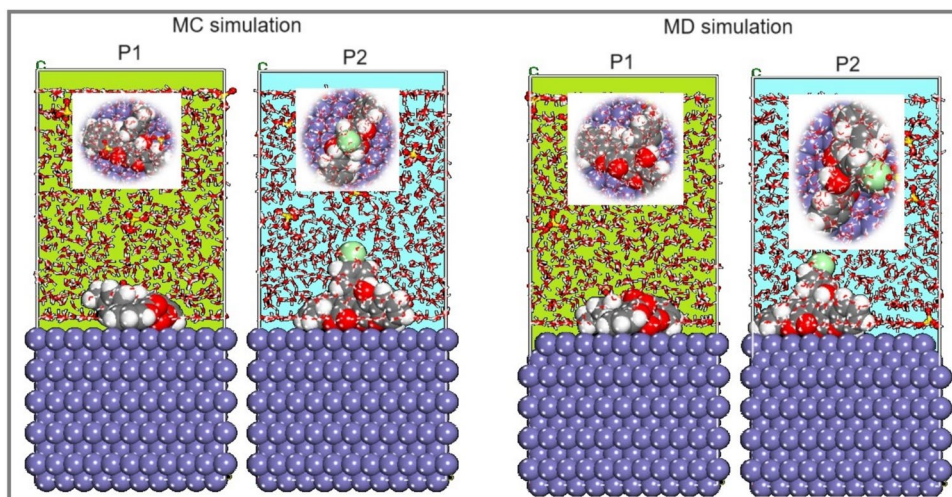
Fig. 16 Distribution of the E_{ads} of inhibitors P1 and P2 on the Iron (Fe) surface

was also investigated. As a result, the goal of this section is to forecast the optimal adsorption sites for both molecules. Table 8 in this idea shows the computed Fukui indices. According to the data in Table 8, the C8, O21, C27, and C29 atoms in P1 have strong positive values of both FI (f_k^+, f_k^-), demonstrating that these centers have a

significant role in the success of the adsorption process to stainless steel.

The P2 has the highest positive values of both FI (f_k^+, f_k^-) and are located on Cl7, C8, O21, C27 and C29.

3.7.2 MC and MD Simulations

Figure 15 illustrates the adsorption characteristics of P1 and P2 inhibitors on the Fe (110) surface in the presence of H_2O and H_2SO_4 molecules. Both inhibitors exhibited parallel adsorption to the Fe (110) surface, maximizing the interaction between their active sites and the metal surface. This parallel orientation effectively covered the entire steel surface. In comparison to water and H_2SO_4 molecules, the organic molecules were positioned closest to the Fe surface (110), suggesting that the presence of organic inhibitors promotes the replacement of H_2O molecules, hydronium ions, and sulfate ions with organic molecules at the electrolyte/metal interface.

The adsorption energies (kcal/mol) are shown in Fig. 16. The figure clearly shows that the Eads of the inhibitors P1 and P2 on the iron surface (110) following the order: P1 (E_{ads} = −221.82 kcal mol^{-1}) > P2 (E_{ads} = −217.15 kcal mol^{-1}). These findings demonstrate that the P1 inhibitor is the most efficient corrosion inhibitor.
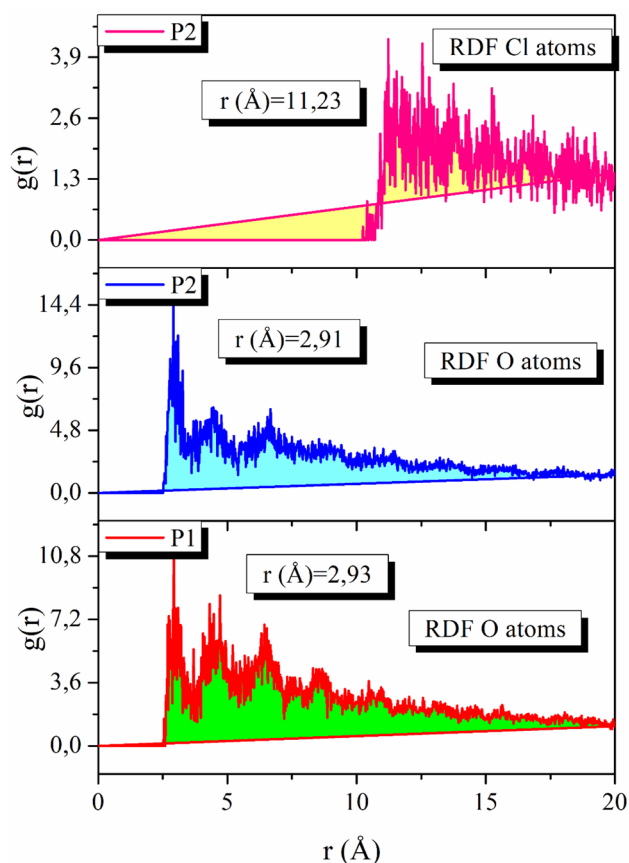
Fig. 17 RDF O and Cl atoms of the P1 and P2 inhibitors in the simulated corrosion media onto Fe surface

Using RDF analysis of the MD trajectory in corrosion simulations as a fundamental tool to examine the adsorption of corrosion inhibitors on metal surfaces [11, 46].

Figure 17 depicts the RDF analysis of heteroatom (O) for inhibitors on the Fe(110) surface, which was determined from MD trajectory analysis. The RDF graph helps to forecast the adsorption process by analyzing peaks at specified distances from the metal surface [94]. Peaks between 1 and 3.5 Å from the surface indicate chemisorption activities, while those above 3.5 Å indicate physical adsorption processes [95]. RDF peaks were found at distances smaller than 3.5 Å for Fe surface heteroatoms (O) (Fe(surface)-P1 (2.93 Å) and Fe(surface)-P2 (2.91 Å). This shows a strong contact between the P1 and P2 inhibitors and the metal surface, as evidenced by the significantly low negative energy values and the presence of conspicuous RDF peaks.

3.8 Adsorption Mechanism

The bibliographic data clearly outlines the well-established mechanism of corrosion inhibition in acidic media [96–100]. It explains that inhibitor molecules adsorb onto
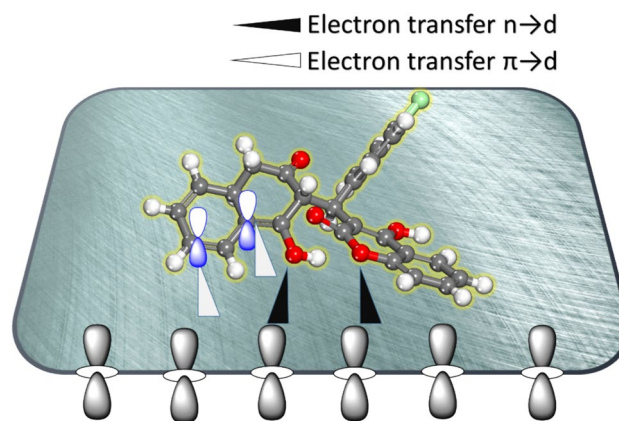

Fig. 18 The schematic depiction of the inhibitors chemisorption mechanism onto Fe surface

metal surfaces through one of four methods: (1) electrostatic attraction between charged molecules and the charged metal, (2) interaction between unshared electron pairs in the inhibitor molecule and the metal, (3) interaction of π-electrons with the metal, or (4) a combination of these methods [101–105]. For physical adsorption to occur in an acidic medium, it is essential to have a metal surface with vacant low-energy electron orbitals and charged species in the solution, such as a molecule with loosely bound electrons or heteroatoms possessing a lone pair of electrons. The adsorbed P1 or P2 molecules may establish a stronger interaction through the formation of coordinate covalent bonds between the oxygen atoms in its aromatic rings and the metal surface. These interactions result in the creation of a protective film on the steel surface, with a large interaction energy, thereby reducing the corrosion rate as demonstrated by experimental results. This organic film acts as a physical barrier, preventing corrosive species from reaching the metal surface (Fig. 18).

4 Conclusion

The purpose of this work was to test the effect of two novel biscoumarin compounds against S-steel corrosion, and the following conclusions were drawn:

– The investigated molecules exhibited outstanding protective properties for S-steel in a 2M H_2SO_4 environment. The inhibition efficiency increased with higher concentrations and exhibited a slight decrease with rising temperature. At 298 K, the maximum protection efficiency reached approximately 98% for P1 at 10^{-3} M and 99% for P2 at the same concentration.

- Polarization plots confirm the mixed-type corrosion inhibition behavior of the investigated compounds.
- EIS measurements reveal an increase in R_p and a decrease in C_{dl} upon the introduction of the two compounds, substantiating the protective capability of the inhibitor molecules.
- The adsorption of these organic compounds adheres to the Langmuir isotherm model.
- The presence of the adsorbed film on the surface of S-steel has been verified through microscopic observations using SEM–EDX.
- According to DFT calculations, the adsorption centers of the P1 and P2 inhibitors are located on the heteroatom. MD and MC calculations show that the P1 and P2 molecules are adsorbed flat on the iron surface, and that the P1 and P2 and metal surface have a strong adsorptive interaction. The experimental findings are corroborated by the theoretical calculations.

Data Availability The data will be made available upon request.

Declarations

Competing interests The authors declare that there are no conflicts of interest.

References

1. Alamry KA, Aslam R, Khan A, Hussein MA, Tashkandi NY (2022) Evaluation of corrosion inhibition performance of thiazolidine-2, 4-diones and its amino derivative: gravimetric, electrochemical, spectroscopic, and surface morphological studies. Process Saf Environ Prot 159:178–197
2. Fernine Y, Arrousse N, Haldhar R, Raorane CJ, Ech-Chihbi E, Kim SC et al (2022) Novel thiophene derivatives as eco-friendly corrosion inhibitors for mild steel in 1 M HCl solution: characterization, electrochemical and computational (DFT and MC simulations) methods. J Environ Chem Eng 10:108891
3. Verma C, Quraishi M, Ebenso EE, Bahadur I (2018) A green and sustainable approach for mild steel acidic corrosion inhibition using leaves extract: experimental and DFT studies. J Bio Tribo-Corros 4:1–12
4. Mouaden KE, Chauhan D, Quraishi M, Bazzi L (2020) Thiocarbohydrazide-crosslinked chitosan as a bioinspired corrosion inhibitor for protection of stainless steel in 3.5% NaCl. Sustain Chem Pharm 15:100213
5. Heakal FET, Fouda A, Radwan M (2011) Inhibitive effect of some thiadiazole derivatives on C-steel corrosion in neutral sodium chloride solution. Mater Chem Phys 125:26–36
6. Wang CL, Guo HD, Fang J, Yu SX, Yue XQ, Hu QH et al (2023) The role of Cr content on the corrosion resistance of carbon steel and low-Cr steels in the CO2-saturated brine. Pet Sci 20:1155–1168
7. Dagdag O, Harfi AE, Essamri A, Bachiri AE, Hajjaji N, Erramli H et al (2018) Anticorrosive performance of new epoxy-amine coatings based on zinc phosphate tetrahydrate as a nontoxic pigment for carbon steel in NaCl medium. Arab J Sci Eng 43:5977–5987
8. Dagdag O, El Harfi A, El Gana L, Hlimi Z, Erramli H, Hamed O et al (2019) The role of zinc phosphate pigment in the anticorrosion properties of bisphenol A diglycidyl ether-polyaminoamide coating for aluminum alloy AA2024-T3. J Bio Tribo-Corros 5:1–10
9. Chiang PC, Chen CW, Tsai FT, Lin CK, Chen CC (2021) Hard anodization film on carbon steel surface by thermal spray and anodization methods. Materials 14:3580
10. Hoshino K, Furuya S, Buchheit RG (2018) Effect of NO^{3-} intercalation on corrosion resistance of conversion coated Zn-Al-CO$_3$ LDHs on electrogalvanized steel. J Electrochem Soc 165:C461
11. Iroha NB, Anadebe VC, Maduelosi NJ, Nnanna LA, Isaiah LC, Dagdag O et al (2023) Linagliptin drug molecule as corrosion inhibitor for mild steel in 1 M HCl solution: electrochemical, SEM/XPS, DFT and MC/MD simulation approach. Colloids Surf, A 660:130885
12. Ganjoo R, Sharma S, Thakur A, Assad H, Sharma PK, Dagdag O et al (2022) Experimental and theoretical study of sodium cocoyl glycinate as corrosion inhibitor for mild steel in hydrochloric acid medium. J Mol Liq 364:119988
13. Erramli H, Dagdag O, Safi Z, Wazzan N, Guo L, Abbout S et al (2020) Trifunctional epoxy resin as anticorrosive material for carbon steel in 1 M HCl: experimental and computational studies. Surfaces Interfaces 21:100707
14. Qiang Y, Zhi H, Guo L, Fu A, Xiang T, Jin Y (2022) Experimental and molecular modeling studies of multi-active tetrazole derivative bearing sulfur linker for protecting steel from corrosion. J Mol Liq 351:118638
15. Qiang Y, Guo L, Li H, Lan X (2021) Fabrication of environmentally friendly Losartan potassium film for corrosion inhibition of mild steel in HCl medium. Chem Eng J 406:126863
16. Eliboev I, Berdimurodov E, Yakhshinorov K, Abdisattarov J, Dagdag O, Berisha A et al (2023) Supramolecular corrosion protection: eco-friendly synthesis and efficacy of β-cyclodextrin/o-phenylenediamine complex. J Taiwan Inst Chem Eng 147:104944
17. Lamghafri S, Daoudi W, El Aatiaoui A, Dagdag O, Berisha A, Barrahi A et al (2023) Comparative study of the performance and inhibitory efficiency of two new organic heterocyclic in the chemical industry. Mater Sci Eng, B 297:116779
18. Salarvand Z, Amirnasr M, Talebian M, Raeissi K, Meghdadi S (2017) Enhanced corrosion resistance of mild steel in 1 M HCl solution by trace amount of 2-phenyl-benzothiazole derivatives: experimental, quantum chemical calculations and molecular dynamics (MD) simulation studies. Corros Sci 114:133–145
19. El Aoufir Y, Lgaz H, Bourazmi H, Kerroum Y, Ramli Y, Guenbour A et al (2016) Quinoxaline derivatives as corrosion

inhibitors of carbon steel in hydrochloridric acid media: electrochemical, DFT and Monte Carlo simulations studies. J Mater Environ Sci 7:4330–4347

20. Obot I, Madhankumar A, Umoren S, Gasem Z (2015) Surface protection of mild steel using benzimidazole derivatives: experimental and theoretical approach. J Adhes Sci Technol 29:2130–2152

21. Verma C, Quraishi M, Ebenso E, Obot I, El Assyry A (2016) 3-Amino alkylated indoles as corrosion inhibitors for mild steel in 1M HCl: experimental and theoretical studies. J Mol Liq 219:647–660

22. Zarrouk A, Hammouti B, Lakhlifi T, Traisnel M, Vezin H, Bentiss F (2015) New 1H-pyrrole-2, 5-dione derivatives as efficient organic inhibitors of carbon steel corrosion in hydrochloric acid medium: electrochemical, XPS and DFT studies. Corros Sci 90:572–584

23. Cherrak K, Benhiba F, Sebbar N, Essassi E, Taleb M, Zarrouk A et al (2019) Corrosion inhibition of mild steel by new Benzothiazine derivative in a hydrochloric acid solution: experimental evaluation and theoretical calculations. Chem Data Collect 22:100252

24. El Azzouzi M, Aouniti A, Tighadouin S, Elmsellem H, Radi S, Hammouti B et al (2016) Some hydrazine derivatives as corrosion inhibitors for mild steel in 1.0 M HCl: weight loss, electrochemichal, SEM and theoretical studies. J Mol Liq 221:633–641

25. Verma C, Saji VS, Quraishi M, Ebenso E (2020) Pyrazole derivatives as environmental benign acid corrosion inhibitors for mild steel: experimental and computational studies. J Mol Liq 298:111943

26. Yang J, Liu GY, Dai F, Cao XY, Kang YF, Hu LM et al (2011) Synthesis and biological evaluation of hydroxylated 3-phenylcoumarins as antioxidants and antiproliferative agents. Bioorg Med Chem Lett 21:6420–6425

27. Peng XM, Damu GLV, Zhou H (2013) Current developments of coumarin compounds in medicinal chemistry. Curr Pharm Des 19:3884–3930

28. Witaicenis A, Seito LN, da Chagas AS, de Almeida Jr LD, Luchini AC, Rodrigues-Orsi P et al (2014) Antioxidant and intestinal anti-inflammatory effects of plant-derived coumarin derivatives. Phytomedicine 21:240–246

29. Nasr T, Bondock S, Youns M (2014) Anticancer activity of new coumarin substituted hydrazide–hydrazone derivatives. Eur J Med Chem 76:539–548

30. Parlak AE, Omar RA, Koparir P, Salih MI (2022) Experimental, DFT and theoretical corrosion study for 4-(((4-ethyl-5-(thiophen-2-yl)-4H-1, 2, 4-triazole-3-yl) thio) methyl)-7, 8-dimethyl-2H-chromen-2-one. Arab J Chem 15:104088

31. Canning C, Sun S, Ji X, Gupta S, Zhou K (2013) Antibacterial and cytotoxic activity of isoprenylated coumarin mammea A/AA isolated from *Mammea africana*. J Ethnopharmacol 147:259–262

32. El Faydy M, Lakhrissi B, Guenbour A, Kaya S, Bentiss F, Warad I et al (2019) In situ synthesis, electrochemical, surface morphological, UV–visible, DFT and Monte Carlo simulations of novel 5-substituted-8-hydroxyquinoline for corrosion protection of carbon steel in a hydrochloric acid solution. J Mol Liq 280:341–359

33. Bentiss F, Outirite M, Traisnel M, Vezin H, Lagrenée M, Hammouti B et al (2012) Improvement of corrosion resistance of carbon steel in hydrochloric acid medium by 3, 6-bis (3-pyridyl) pyridazine. Int J Electrochem Sci 7:1699–1723

34. Dagdag O, El Harfi A, Safi Z, Guo L, Kaya S, Verma C et al (2020) Cyclotriphosphazene based dendrimeric epoxy resin as an anti-corrosive material for copper in 3% NaCl: experimental and computational demonstrations. J Mol Liq 308:113020

35. Abdellattif MH, Alrefaee SH, Dagdag O, Verma C, Quraishi M (2021) Calotropis procera extract as an environmental friendly corrosion inhibitor: computational demonstrations. J Mol Liq 337:116954

36. Bhardwaj N, Sharma P, Guo L, Dagdag O, Kumar V (2022) Molecular dynamic simulation, quantum chemical calculation and electrochemical behaviour of *Punica granatum* peel extract as eco-friendly corrosion inhibitor for stainless steel (SS-410) in acidic medium. J Mol Liq 346:118237

37. Yukna RA, Callan DP, Krauser JT, Evans GH, Aichelmann-Reidy ME, Moore K et al (1998) Multi-center clinical evaluation of combination anorganic bovine-derived hydroxyapatite matrix (ABM)/cell binding peptide (P-15) as a bone replacement graft material in human periodontal osseous defects. 6-month results. J Periodontol 69:655–663

38. Andzelm J, King-Smith R, Fitzgerald G (2001) Geometry optimization of solids using delocalized internal coordinates. Chem Phys Lett 335:321–326

39. Inada Y, Orita H (2008) Efficiency of numerical basis sets for predicting the binding energies of hydrogen bonded complexes: evidence of small basis set superposition error compared to Gaussian basis sets. J Comput Chem 29:225–232

40. Daoudi W, El Ibrahimi B, Dagdag O, Berdimurodov E, Guo L, Ebenso EE et al (2023) New chlorophenyl-imidazole derivative as a novel corrosion inhibitor in the gas and oil industry. J Phys Chem Solids 179:111409

41. Gupta SK, Mehta RK, Yadav M, Dagdag O, Mehmeti V, Berisha A et al (2023) Diazenyl derivatives as efficient corrosion inhibitors for mild steel in HCl medium: gravimetric, electrochemical and computational approach. J Mol Liq 382:121976

42. Ihamdane R, Tiskar M, Outemsaa B, Zelmat L, Dagdag O, Berisha A et al (2023) Essential oil of *Origanum vulgare* as a green corrosion inhibitor for carbon steel in acidic medium. Arab J Sci Eng. https://doi.org/10.1007/s13369-023-07693-0

43. Dagdag O, El Harfi A, El Gana L, Safi ZS, Guo L, Berisha A et al (2021) Designing of phosphorous based highly functional dendrimeric macromolecular resin as an effective coating material for carbon steel in NaCl: computational and experimental studies. J Appl Polym Sci 2021:49673

44. Haldhar R, Vanaraj R, Dagdag O, Berisha A, Kim S-C (2023) *Convolvulus microphyllus* extract as a green, effective, and affordable corrosion inhibitor: theoretical calculations and experimental studies. Coatings 13:860

45. Daoudi W, Azzouzi M, Dagdag O, El Boutaybi A, Berisha A, Ebenso EE et al (2023) Synthesis, characterization, and corrosion inhibition activity of new imidazo [1.2-a] pyridine chalcones. Mater Sci Eng, B 290:116287

46. Dagdag O, Haldhar R, Kim SC, Safi ZS, Wazzan N, Mkadmh AM et al (2022) Synthesis, physicochemical properties, theoretical and electrochemical studies of tetraglycidyl methylenedianiline. J Mol Struct 1265:133508

47. Ashassi-Sorkhabi H, Ghalebsaz-Jeddi N, Hashemzadeh F, Jahani H (2006) Corrosion inhibition of carbon steel in hydrochloric acid by some polyethylene glycols. Electrochim Acta 51:3848–3854

48. Hmamou DB, Salghi R, Zarrouk A, Zarrok H, Touzani R, Hammouti B et al (2015) Investigation of corrosion inhibition of carbon steel in 0.5 M H_2SO_4 by new bipyrazole derivative using experimental and theoretical approaches. J Environ Chem Eng 3:2031–2041

49. Dastgerdi AA, Brenna A, Ormellese M, Pedeferri M, Bolzoni F (2019) Experimental design to study the influence of temperature, pH, and chloride concentration on the pitting and crevice corrosion of UNS S30403 stainless steel. Corros Sci 159:108160

50. Esmailzadeh S, Aliofkhazraei M, Sarlak H (2018) Interpretation of cyclic potentiodynamic polarization test results for study of corrosion behavior of metals: a review. Prot Met Phys Chem Surf 54:976–989

51. Wilde B, Williams E (1971) The use of current/voltage curves for the study of localized corrosion and passivity breakdown on stainless steels in chloride media. Electrochim Acta. https://doi.org/10.1016/0013-4686(71)85151-4

52. Obot I, Solomon M, Onyeachu I, Umoren S, Meroufel A, Alenazi A et al (2020) Development of a green corrosion inhibitor for use in acid cleaning of MSF desalination plant. Desalination 495:114675

53. Fekry A, Ameer M (2010) Corrosion inhibition of mild steel in acidic media using newly synthesized heterocyclic organic molecules. Int J Hydrogen Energy 35:7641–7651

54. Yadav M, Kumar S, Sharma D, Yadav P (2013) Experimental and quantum studies on adsorption and corrosion inhibition effect of imidazole derivatives on N 80 steel in hydrochloric acid. Surf Rev Lett 20:1350057

55. Bai L, Feng LJ, Wang HY, Lu YB, Lei XW, Bai FL (2015) Comparison of the synergistic effect of counterions on the inhibition of mild steel corrosion in acid solution: electrochemical, gravimetric and thermodynamic studies. RSC Adv 5:4716–4726

56. Labjar N, Lebrini M, Bentiss F, Chihib N-E, El Hajjaji S, Jama C (2010) Corrosion inhibition of carbon steel and antibacterial properties of aminotris-(methylenephosphonic) acid. Mater Chem Phys 119:330–336

57. Chahmout H, Ouakki M, Sibous S, Galai M, Arrousse N, Ech-chihbi E et al (2023) New pyrazole compounds as a corrosion inhibitor of stainless steel in 2.0 M H_2SO_4 medium: electrochemical and theoretical insights. Inorg Chem Commun 147:110150

58. Raviprabha K, Bhat RS (2019) 5-(3-Pryridyl)-4H-1, 2, 4-triazole-3-thiol as potential corrosion inhibitor for AA6061 aluminium alloy in 0.1 M hydrochloric acid solution. Surf Eng Appl Electrochem 55:723–733

59. Priya AS, Muralidharan V, Subramania A (2008) Erratum: Development of novel acidizing inhibitors for carbon steel corrosion in 15% boiling hydrochloric acid (vol. 64, No. 6, p. 541–552). Corrosion 64:687

60. Rehim SSA, Hassan HH, Amin MA (2002) Corrosion and corrosion inhibition of Al and some alloys in sulphate solutions containing halide ions investigated by an impedance technique. Appl Surf Sci 187:279–290

61. Popova A, Christov M (2006) Evaluation of impedance measurements on mild steel corrosion in acid media in the presence of heterocyclic compounds. Corros Sci 48:3208–3221

62. Wang Q, Zhou X, Wang R, Aslam R, Sun X, Sun Y et al (2024) Synergistic effect of KI on corrosion inhibition of carbon steel by *Styphnolobium japonicum* (L.) Schott in H_2SO_4 solution. J Mol Struct 1309:138251

63. Haldhar R, Prasad D, Saharan H (2020) Performance of *Pfaffia paniculata* extract towards corrosion mitigation of low-carbon steel in an acidic environment. Int J Ind Chem 11:1–12

64. Hegazy M, Abdallah M, Awad M, Rezk M (2014) Three novel di-quaternary ammonium salts as corrosion inhibitors for API X65 steel pipeline in acidic solution. Part I: experimental results. Corros Sci 81:54–64

65. Rbaa M, Ouakki M, Galai M, Berisha A, Lakhrissi B, Jama C et al (2020) Simple preparation and characterization of novel 8-Hydroxyquinoline derivatives as effective acid corrosion inhibitor for mild steel: experimental and theoretical studies. Colloids Surf, A 602:125094

66. Wang Q, Wang R, Sun X, Aslam R, Zhou X, Zhang Q et al (2024) Protein-derived carbon dots as green corrosion inhibitors for carbon steel in sulfuric acid solution. Diam Relat Mater 145:111135

67. Hsu C, Mansfeld F (2001) Concerning the conversion of the constant phase element parameter Y0 into a capacitance. Corrosion 57:747

68. Yadav DK, Quraishi MA (2012) Application of some condensed uracils as corrosion inhibitors for mild steel: gravimetric, electrochemical, surface morphological, UV–visible, and theoretical investigations. Ind Eng Chem Res 51:14966–14979

69. Ouakki M, Galai M, Rbaa M, Abousalem A, Lakhrissi B, Rifi E et al (2019) Quantum chemical and experimental evaluation of the inhibitory action of two imidazole derivatives on mild steel corrosion in sulphuric acid medium. Heliyon. https://doi.org/10.1016/j.heliyon.2019.e02759

70. Ren Y, Zhang J, Du M, Niu L (2016) The synergistic inhibition effect between imidazoline-based dissymmetric bis-quaternary ammonium salts and thiourea on Q235 steel in CO_2 corrosion process. Res Chem Intermed 42:641–657

71. Khalid Al-Azzawi W, Hussein SS, Salih SM, Zinad D, Al-Azzawi R, Hanoon M et al (2023) Efficient protection of mild steel corrosion in hydrochloric acid using 3-(5-amino-1, 3, 4-thiadiazole-2yl)-2H-chromen-2-one, a coumarin derivative bearing a 1, 3, 4-thiadiazole moiety: Gravimetrical techniques, computational and thermodynamic investigations. Prog Color Colorants Coat 16:97–111

72. Verma DK, Kaya S, Ech-chihbi E, El-Hajjaji F, Phukan MM, Alnashiri HM (2021) Investigations on some coumarin based corrosion inhibitors for mild steel in aqueous acidic medium: electrochemical, surface morphological, density functional theory and Monte Carlo simulation approach. J Mol Liq 329:115531

73. Mahalakshmi D, Hemapriya V, Subramaniam EP, Chitra S (2019) Synergistic effect of antibiotics on the inhibition property of aminothiazolyl coumarin for corrosion of mild steel in 0.5 M H_2SO_4. J Mol Liq 284:316–327

74. El-Raouf MA, Khamis E, Abou Kana MT, Negm NA (2018) Electrochemical and quantum chemical evaluation of new bis (coumarins) derivatives as corrosion inhibitors for carbon steel corrosion in 05 M H_2SO_4. J Mol Liquids 255:341–353

75. Fergachi O, Benhiba F, Rbaa M, Ouakki M, Galai M, Touir R et al (2019) Corrosion inhibition of ordinary steel in 5.0 M HCl medium by benzimidazole derivatives: electrochemical, UV–visible spectrometry, and DFT calculations. J Bio- Tribo-Corros 5:1–13

76. Mobin M, Aslam R, Salim R, Kaya S (2022) An investigation on the synthesis, characterization and anti-corrosion properties of choline based ionic liquids as novel and environmentally friendly inhibitors for mild steel corrosion in 5% HCl. J Colloid Interface Sci 620:293–312

77. Hisham J, Elsousy KM, Hartany KA (2016) Kinetics, equilibrium, and isotherm of the adsorption of cyanide by MDFSD. Arab J Chem 9:S198–S203

78. Khamis E, Abd-El-Khalek D, Abdel-Kawi MA, Anwar J (2022) New application of brown sea algae as an alternative to phosphorous-containing antiscalant. Environ Technol 43:595–604

79. Fouda A, Gadow H, Abd Elal E, El-Tantawy M (2021) Corrosion inhibition of aluminium by rice straw extract in 2 M hydrochloric acid solution. J Bio Tribo-Corros 7:102

80. Sedik A, Lerari D, Salci A, Athmani S, Bachari K, Gecibesler İ et al (2020) Dardagan Fruit extract as eco-friendly corrosion inhibitor for mild steel in 1 M HCl: electrochemical and surface morphological studies. J Taiwan Inst Chem Eng 107:189–200

81. Singh P, Chauhan D, Chauhan S, Singh G, Quraishi M (2020) Bioinspired synergistic formulation from dihydropyrimdinones and iodide ions for corrosion inhibition of carbon steel in sulphuric acid. J Mol Liq 298:112051

82. Elbarki A, Guerrab W, Laabaissi T, Benhiba F, Rouifi Z, Oudda H et al (2020) Chemical, electrochemical and theoretical studies of 3-methyl-5, 5′-diphenylimidazolidine-2, 4-dione as corrosion inhibitor for mild steel in HCl solution. Chem Data Collect 28:100454

83. Ammar I, El Khorafi F (1973) Adsorbability of thiourea on iron cathodes. Mater Corros 24:702–707

84. Benhiba F, Benzekri Z, Guenbour A, Tabyaoui M, Bellaouchou A, Boukhris S et al (2020) Combined electronic/atomic level computational, surface (SEM/EDS), chemical and electrochemical studies of the mild steel surface by quinoxalines derivatives anti-corrosion properties in 1 mol· L-1 HCl solution. Chin J Chem Eng 28:1436–1458

85. Fernine Y, Arrousse N, Haldhar R, Raorane CJ, Kim SC, El Hajjaji F et al (2022) Synthesis and characterization of phenolphthalein derivatives, detailed theoretical DFT computation/molecular simulation, and prevention of AA2024-T3 corrosion in medium 3.5% NaCl. J Taiwan Inst Chem Eng 140:104556

86. Ihamdane R, Tiskar M, Outemsaa B, Zelmat L, Dagdag O, Berisha A et al (2023) Essential oil of *Origanum vulgare* as a green corrosion inhibitor for carbon steel in acidic medium. Arab J Sci Eng 48:1–17

87. Dagdag O, El Harfi A, El Gana L, Safi ZS, Guo L, Berisha A et al (2021) Designing of phosphorous based highly functional dendrimeric macromolecular resin as an effective coating material for carbon steel in NaCl: computational and experimental studies. J Appl Polym Sci 138:49673

88. Bhardwaj N, Sharma P, Guo L, Dagdag O, Kumar V (2022) Molecular dynamic simulation and Quantum chemical calculation of phytochemicals present in *Beta vulgaris* and electrochemical behaviour of Beta vulgaris peel extract as green corrosion inhibitor for stainless steel (SS-410) in acidic medium. Colloids Surf A 632:127707

89. Berdimurodov E, Kholikov A, Akbarov K, Guo L, Kaya S, Katin KP et al (2022) Novel cucurbit [6] uril-based [3] rotaxane supramolecular ionic liquid as a green and excellent corrosion inhibitor for the chemical industry. Colloids Surf A 633:127837

90. Haldhar R, Prasad D, Kamboj D, Kaya S, Dagdag O, Guo L (2021) Corrosion inhibition, surface adsorption and computational studies of Momordica charantia extract: a sustainable and green approach. SN Applied Sciences 3:1–13

91. Berdimurodov E, Kholikov A, Akbarov K, Guo L, Kaya S, Verma DK et al (2022) Novel glycoluril pharmaceutically active compound as a green corrosion inhibitor for the oil and gas industry. J Electroanal Chem 907:116055

92. Aslam R, Mobin M, Shoeb MH, Murmu M, Banerjee P (2021) Proline nitrate ionic liquid as high temperature acid corrosion inhibitor for mild steel: experimental and molecular-level insights. J Ind Eng Chem 100:333–350

93. Nnaji N, Sen P, Openda YI, Berisha A, Dagdag O, Ebenso EE et al (2023) Assessing the potentials of free base and gallium metalated tertbutylphthalocyanines as aluminium corrosion inhibitors. Int J Electrochem Sci 2023:100345

94. Daoudi W, El Aatiaoui A, Falil N, Azzouzi M, Berisha A, Olasunkanmi LO et al (2022) Essential oil of Dysphania ambrosioides as a green corrosion inhibitor for mild steel in HCl solution. J Mol Liq 363:119839

95. Gupta SK, Mitra R, Yadav M, Dagdag O, Berisha A, Mamba BB et al (2023) Electrochemical, surface morphological and computational evaluation on carbohydrazide Schiff bases as corrosion inhibitor for mild steel in acidic medium. Sci Rep 13:15108

96. Berisha A, Hadhlar R, Dagdag O (2024) Ab initio exploration of modified carbon nanotubes as potential corrosion inhibitors. Maced J Chem Chem Eng 43:115–126

97. El-Aouni N, Dagdag O, El-Amri A, Kim H, Haldhar R, Kim SC et al (2024) Study of new phosphorus-sulfur epoxy polymer for CS anticorrosion in HCl solution: experimental and theoretical investigations. Mater Sci Eng, B 299:117011

98. El Mahamdi M, Daoudi W, Dagdag O, Kim H, Eddaoudy F, Verma DK et al (2023) Integrating experimental and theoretical studies in the development of a novel alginate-based biocomposite for copper anticorrosion in 3.5% NaCl environments. Int J Biol Macromol 2023:128600

99. El-Aouni N, Dagdag O, El Amri A, Berradi M, Kim H, Elbachiri A et al (2024) Experimental and computational insights into destruction protection of E24 carbon metal by new trifunctional sulfur-phosphorus epoxy polymer. J Taiwan Inst Chem Eng 155:105281

100. Ran B, Qiang Y, Liu X, Guo L, Ritacca AG, Ritacco I et al (2024) Excellent performance of amoxicillin and potassium iodide as hybrid corrosion inhibitor for mild steel in HCl environment: adsorption characteristics and mechanism insight. J Mater Res Technol 29:5402

101. El-Aouni N, Dagdag O, El Amri A, Kim H, Elbachiri A, Berdimurodov E et al (2024) Innovative phosphorus-containing epoxy resins: A new approach to acidic corrosion protection. Colloids Surfaces A Physicochem Eng Aspects 2024:133730

102. Abouchane M, Hsissou R, Chraka A, Molhi A, Damej M, Tassaoui K et al (2024) Synthesis and characterization of new macromolecular epoxy resin as an effective corrosion inhibitor for C38 steel in 1 M HCl medium: electrochemical insights, surface morphological and computational approaches. J Bio Tribo-Corros 10:21

103. Daoudi W, Dagdag O, Verma C, Berdimurodov E, Oussaid A, Berisha A et al (2024) Rosmarinus officinalis l. Oil as an eco-friendly corrosion inhibitor for mild steel in acidic solution: experimental and computational studies. Inorg Chem Commun 161:112030

104. Lamghafri S, Daoudi W, El Aatiaoui A, Dagdag O, Kim H, Benhiba F et al (2024) Performance of *Artemisia absinthium* as an ecological corrosion inhibitor in the industrial pickling process. J Bio Tribo-Corros 10:17

105. Dadou S, Elyoussfi A, Dagdag O, Koudad M, Isaad J, Kim H et al (2024) The impact of halogen substitution on the corrosion inhibition of imidazothiazole derivatives for mild steel in corrosive media (Part A). Colloids Surfaces A Physicochem Eng Aspects 2024:133451